On the Determination of the Roughness of Metallic Surfaces[1]

CARL WAGNER[2]

Eduard Zintl Institut fuer anorganische und physikalische Chemie der Technischen Hochschule Darmstadt, Germany

ABSTRACT

It is shown that the polarization capacity of an electrode can be measured readily with the aid of a ballistic galvanometer. The polarization capacity per unit apparent area can be considered to be approximately proportional to the roughness of the surface of the electrode. Results obtained on silver electrodes illustrate the influence of pretreatment and aging.

INTRODUCTION

It is known that the true surface area of a solid frequently exceeds by far its geometrical or apparent surface area because of a certain "roughness." To characterize a surface quantitatively, a roughness factor may be defined as ratio of the true surface area to the apparent surface area. In the case of solid catalysts the true surface area may be determined with the aid of adsorption measurements as shown, e.g., by Emmett and Brunauer (1). Other methods and the principal difficulties of defining surface areas have recently been surveyed by Zimens (2) and Bikerman (3). Bowden and Rideal (4, 5) have indicated a method which rests on the measurement of the polarization capacity of a metallic surface immersed in an aqueous solution. This method seems to be of special value when one wants to determine the roughness of electrodeposited coatings and corroding metals because this method can also be used in the case of small areas and the measurement can virtually be made under the conditions of immediate interest. No essential change of the state of the surface owing to the measuring procedure is to be expected.

When the intensity of the current flowing from a metal to an adjacent aqueous solution is suddenly increased, the electrical potential difference between metal and aqueous solution also changes but there is a time delay due to the fact that a different potential difference between metal and aqueous solution involves a different structure of the boundary layer, and a change of the number of electrically charged particles at either side of the electrical double layer requires a finite quantity of electricity flowing through the system. Theoretical relations have been reviewed by Butler (6).

The behavior of an electrode resembles that of a resistance with a capacity in parallel as shown by Kohlrausch (7) and others. Several methods have been developed in order to determine the magnitude of the "polarization capacity," which is defined as capacity in the aforementioned equivalent circuit. For instance, one can evaluate observations of the potential-time relation after a sudden increase of the current (5, 8, 10, 11), or one can make bridge measurements with alternating current (12–20). Some authors, who applied alternating current, assumed an equivalent circuit consisting of a resistance and a capacity in series; the magnitude of a capacity defined in this manner can differ widely from that corresponding to the aforementioned definition. The possibility of a difference in definition must be borne in mind when numerical values obtained by means of different methods are compared with each other.

Bowden and Rideal (4, 5) chose conditions under which the steady-state current flowing through the electrode practically vanishes. These authors employed solutions free from substances reducible in the potential range applied. For instance, silver was placed in a solution free from silver ions and oxygen, and the potential was kept within such limits that hydrogen gas was not evolved. In the initial state, the potential of the electrode against a reference electrode was given a defined value with the aid of a potentiometer and it was ascertained that the current flowing through the system practically vanished. Then a d-c current of given strength I was applied and the resulting change ΔE of the potential was observed as a function of time t. The polarization capacity C per unit apparent area can be calculated as follows:

$$C = \frac{I}{A}\frac{\Delta t}{\Delta E} \qquad (1)$$

where A is the apparent surface area of the electrode.

Bowden and Rideal (5) found a polarization capacity of liquid mercury in dilute sulfuric acid of 6 $\mu F/cm^2$. This value, however, seems to be too low. Recently, Bowden and Grew (21) reported a value

[1] Manuscript received May 24, 1949. This paper prepared for delivery before the Cleveland Meeting, April 19 to 22, 1950.

[2] Present address: Department of Metallurgy, Massachusetts Institute of Technology, Cambridge Massachusetts.

UMI

of 20 $\mu F/cm^2$. Moreover, Bowden and Rideal (5) investigated silver electrodes and obtained polarization capacities ranging from 100 to 310 $\mu F/cm^2$, depending on the previous treatment; the polarization capacity of amalgamated silver was about that of mercury. On platinized platinum a value as high as 11,000 $\mu F/cm^2$ was observed, whereas the value of smooth platinum was only 13 $\mu F/cm^2$.

Bowden and O'Connor (22) investigated a eutectic mixture of bismuth, lead, tin, and cadmium. The polarization capacities of the molten and the solidified alloy, respectively, were as 1 to 1.4. Rubbing the solid alloy with sandpaper caused an increase by a factor of 6. Etching with nitric acid produced a black spongy surface and the polarization capacity increased by a factor of 800 to 1,000.

Moreover, the method of Bowden and Rideal has been used in extensive investigations on platinum electrodes by Slygin and Frumkin (23), Ershler and Proskurnin (24), Ershler (25), and Slygin and Ershler (26). Kabanov, Jofa, and Yudkevich (27, 28) have made measurements on lead electrodes, and Vesolovskii (29) has investigated silver electrodes.

Bowden and Rideal (5) have calculated roughness factors by assuming that the polarization capacity of ideally smooth metallic surfaces is essentially independent of their chemical nature and, therefore, can be set approximately equal to that of mercury. This assumption, however, does not seem quite satisfactory in view of the dependence of the polarization capacity on potential and composition of the adjacent solution. Yudkevich concludes from his measurements that a smooth silver electrode has a polarization capacity as high as 100 $\mu F/cm^2$, but it must be borne in mind that it is difficult to prepare an ideally smooth metallic surface.

In view of these uncertainties it seems preferable to calculate only relative changes of surface areas from measurements of the polarization capacity. If the absolute value of the roughness of a surface is to be determined, other methods should be used. For instance, Brown and Uhlig (30) have adapted the adsorption method to the investigation of samples with apparent surface areas as small as 150 cm^2 and thus were able to make measurements on chromium coatings on nickel.

The measuring method of Bowden and Rideal requires expensive and sensitive equipment and the electrolyte must be thoroughly freed from oxygen and other reducible substances. To simplify measurements and to obtain results also under less favorable conditions, another method seems desirable. Such a method and some characteristic results are reported below.

Experimental

The method suggested in this paper rests on the measurement of the current-time integral for a given change of the potential with the aid of a ballistic galvanometer. This principle was used by Varley (31), Herwig (32), Colley (33), Blondlot (34), Bouty (35), and Lietzau (36) as early as fifty to seventy-five years ago. It is also assumed that in the potential range employed the steady-state current practically vanishes but the requirement is far less severe than for the method of Bowden and associates. The basic set-up is shown in Fig. 1. In the beginning, switch S is open so that the voltage furnished by the potentiometer P_2 is equal to zero, but an initial potential may be applied with the

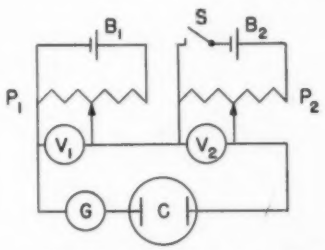

Fig. 1. Set-up for measurement of polarization capacity. B_1, B_2—storage batteries; P_1, P_2—potentiometers; V_1, V_2—voltmeters; S—switch; G—ballistic galvanometer; C—electrolytic cell with measuring electrode and reference electrode.

aid of the potentiometer P_1. Then switch S is closed and thereby an additional voltage indicated by voltmeter V_2 is applied. The current-time integral is obtained from the maximum deflection of the ballistic galvanometer G, the sensitivity of which is appropriately reduced by a shunt in parallel. Since for a surface area of 1 cm^2 the current-time integral is rather large, a portable galvanometer with not too small a time constant can be used. The polarization capacity is calculated from Equation (I) by replacing the product of current and time by the corresponding integral.

Upon opening switch S, a second determination involving the reverse change of the polarization state can be made. It has been ascertained that both kinds of measurements yield practically identical values.

To obtain correct results, the time constant of the measuring circuit must be much less than the time constant of the ballistic galvanometer. This can easily be achieved, for the resistance of the measuring circuit can easily be made less than 50 ohms and then its time constant is low; even in the case of a polarization capacity of 2,000 μF, it is less than 0.05 second.

Measurements were made on silver wires which

were first coated with silver chloride by anodic polarization in chloride solution and then reduced by cathodic polarization. A second silver electrode coated with silver chloride was used as reversible reference electrode. The electrolyte contained 0.25 mole of sodium chloride, 1 mole of acetic acid, and 1 mole of sodium acetate in 1,000 ml of water. Test cells were sealed after the oxygen had been removed from the solution by adding a small amount of sodium bicarbonate which, by reaction with the acetic acid present, formed carbon dioxide which swept oxygen from the solution and the electrode vessel.

TABLE I. *Polarization capacity of a silver electrode as a function of potential against a Ag-AgCl reference electrode*

Potential interval (volt)	Polarization capacity ($\mu F/cm^2$)
0 to −0.1	350
−0.1 to −0.2	330
−0.2 to −0.3	280
−0.3 to −0.4	360
−0.4 to −0.5	520
−0.5 to −0.6	630
−0.6 to −0.7	680

TABLE II. *Polarization capacity of a silver electrode after reduction of the silver-chloride layer**

Time in seconds after reduction of AgCl layer	Polarization capacity for reducing current densities of					
	0.7	1.3	3	4	5	11 milliamp/cm²
						$\mu F/cm^2$
15	280	360	420	450	500	1700
30	280	340	360	360	400	480
45	270	330	350	360	380	430
60	270	320	350	320	360	410
120	260	310	320	320	320	400
600	—	280	270	260	280	310

* The silver-chloride layer was produced by anodic polarization with a current density of 1.3 milliamp/cm² during 180 seconds and was reduced to silver by cathodic polarization with current densities indicated above. To determine the polarization capacity, the potential was changed from 0 to −0.5 volt.

Data compiled in Table I show the dependency of the polarization capacity on the potential of the measuring electrode. This dependency is analogous to that of mercury in various electrolytes (37).

Table II shows the influence of pretreatment. The thickness of the silver-chloride layer was the same in all runs, but the strength of the reducing current was varied, and repeated measurements of the polarization capacity at different times after the end of the reduction process were made in order to obtain information on the aging of the surface. In accordance with the experience of other investigators, the polarization capacity and thus the roughness increases with increasing strength of the reducing current, i.e., with increasing rate of the reduction process. The subsequent aging proceeds mainly within a fraction of a minute; after five minutes virtually no difference between runs involving different reducing currents is noticeable.

It was confirmed that the polarization capacity determined with the aid of a ballistic galvanometer was in accordance with observations of the potential as a function of time when a constant current was applied. But the latter measurements were only incidental and, therefore, not very accurate.

Further tests were performed on silver wires which had not been covered with silver chloride but only cleaned by treating as cathode in a solution of sodium hydroxide, sodium cyanide, and ammonium chloride. Under these conditions a polarization capacity as low as 100 $\mu F/cm^2$ between −0.1 and −0.5 volt was observed. The same value has been reported by Vesolovskii (29) for "smooth" silver electrodes.

If the latter value is assumed to be characteristic of an ideally smooth silver surface, roughness factors as defined above could be calculated by dividing the numerical values of the polarization capacity in $\mu F/cm^2$ by 100. Such a calculation, however, gives only minimum values of roughness factors, since there is no clear-cut proof that a fresh silver wire is ideally smooth.

Conclusions

The foregoing experiments show the applicability of the ballistic galvanometer to determine polarization capacities of electrodes. Measurements were made in connection with the development of an electrolytic integrimeter, which has been described by Moore (38). It can be shown that the ultimate accuracy of this integrimeter is determined by the magnitude of the polarization capacity of the silver electrode used therein.

Any discussion of this paper will appear in a Discussion Section, to be published in the December 1950 issue of the Journal.

REFERENCES

1. P. H. Emmett and S. Brunauer, *J. Am. Chem. Soc.*, **59,** 310, 1553 (1937); P. H. Emmett, *Ind. Eng. Chem.*, **37,** 639 (1945).
2. K. E. Zimens, "Poroese Stoffe. Handbuch der Katalyse," Vol. **4**. Edited by G. M. Schwab, J. Springer, Wien (1944).
3. J. J. Bikermann, "Surface Chemistry for Industrial Research," pp. 167–179, 200–205, 293–300, Academic Press, New York (1948).
4. F. P. Bowden and E. K. Rideal, *Proc. Roy. Soc. London*, **120A,** 59 (1928).

5. F. P. Bowden and E. K. Rideal, *Proc. Roy. Soc. London*, **120A**, 80 (1928).
6. J. A. V. Butler, "Electrocapillarity," pp. 56–91. Chemical Publishing Co., New York (1940).
7. F. Kohlrausch, *Poggendorf's Ann. Physik*, **148**, 443 (1872).
8. M. Le Blanc, "Die electromotorischen Kraefte der Polarization," Knapp, Halle (1910).
9. E. Newberry, *Proc. Roy. Soc. London*, **107A**, 486 (1925); **111A**, 182 (1926); **114A**, 103 (1927).
10. T. Erdey-Grusz and G. Kromvey, *Z. physik. Chem.*, **157A**, 213 (1931).
11. K. F. Bonhoeffer and E. Otto, *Z. physik. Chem.*, **186A**, 248 (1940).
12. W. Nernst, *Z. physik. Chem.*, **14**, 622 (1894).
13. M. Wien, *Wiedemann's Ann. Physik*, **58**, 37 (1896).
14. E. Orlich, Thesis, Berlin (1896).
15. C. M. Gordon, *Wiedemann's Ann. Physik*, **61**, 1 (1897).
16. A. M. Scott, *Wiedemann's Ann. Physik*, **67**, 388 (1899).
17. E. Warburg, *Wiedemann's Ann. Physik*, **67**, 493 (1899).
18. E. Neumann, *Wiedemann's Ann. Physik*, **67**, 500 (1899).
19. F. Krueger, *Z. physik. Chem.*, **45**, 1 (1903).
20. T. Borissa and M. Proskurnin, *Acta Physicochim. U.R.S.S.*, **4**, 819 (1936); **12**, 371 (1940).
21. F. P. Bowden and K. E. W. Grew, "Discussions of the Faraday Society No. 1 (Electrode Processes)," p. 91. Gurney and Jackson, London (1947).
22. F. P. Bowden and E. A. O'Connor, *Proc. Roy. Soc. London*, **127A**, 317 (1930).
23. A. Slygin and A. Frumkin, *Acta Physicochim. U.R.S.S.*, **3**, 791 (1935).
24. B. Ershler and M. Proskurnin, *Acta Physicochim. U.R.S.S.*, **6**, 195 (1937).
25. B. Ershler, *Acta Physicochim. U.R.S.S.*, **7**, 327 (1937).
26. A. Slygin and B. Ershler, *Acta Physicochim. U.R.S.S.*, **11**, 45 (1939).
27. B. Kabanov and S. Jofa, *Acta Physicochim. U.R.S.S.*, **10**, 617 (1939).
28. B. Kabanov and R. Yudkevich, *J. Phys. Chem. U.S.S.R.*, **13**, 813 (1939).
29. V. I. Vesolovskii, *Acta Physicochim. U.R.S.S.*, **11**, 815 (1939).
30. C. Brown and H. H. Uhlig, *J. Am. Chem. Soc.*, **69**, 462 (1947).
31. C. F. Varley, *Phil. Trans.*, **161**, 129 (1872).
32. H. Herwig, *Wiedemann's Ann. Physik*, **2**, 566 (1877).
33. R. Colley, *Wiedemann's Ann. Physik*, **7**, 206 (1879).
34. B. Blondlot, *J. Physique* (1) **10**, 279 (1881).
35. E. Bouty, *Ann. chim. phys.* (6) **3**, 145 (1894).
36. W. Lietzau, *Wiedemann's Ann. Physik*, **55**, 338 (1895).
37. J. A. V. Butler, "Electrocapillarity," pp. 67–69, Chemical Publishing Co., New York (1940).
38. T. M. Moore, *Elec. Eng.*, **65**, 303 (1946); **68**, (1949).

A Unified Mechanism of Passivity and Inhibition. Part II[1]

R. B. MEARS

Research Laboratory, Carnegie-Illinois Steel Corporation, Pittsburgh, Pennsylvania

AND

R. H. BROWN

Aluminum Research Laboratories, Aluminum Company of America, New Kensington, Pennsylvania

ABSTRACT

It is shown that the inhibiting action of sodium chromate on localized corrosion of aluminum exposed to a sodium chloride solution is mainly the result of polarization of the local anodes. Sodium chromate would be an even more effective inhibitor of corrosion in this case if it did not depolarize the local cathodes. In order to obtain dependable information on the mechanism of inhibitor action, the influence of the inhibitor on the behavior of the local cells must be studied. Polarization curves obtained by the use of currents from an external source are of value in studying the mechanism of inhibitor action only if information on local cell behavior can be derived from them. Two indirect methods of estimating the anodic and cathodic polarization curves of the local cells are described. These methods make it possible to obtain the local cell polarization curves without the necessity of locating or isolating the local anodes and cathodes. The practical application of these methods is limited by the assumption that the areas of the local anodes and cathodes are not altered by the application of external current. One of the two methods has additional limitations.

The relationship of "reversible" potentials of metals as calculated from free energy data and as measured in aqueous solutions is discussed. It is indicated that polarization plays an important role in the measurement of potentials commonly accepted as reversible. Agreement between potentials calculated from free energy data and measured "reversible" potentials is dependent upon local cell action of a specific nature. Departure from this specific local cell action accounts for the fact that the measured value of the apparent single potential does not, in most cases, correspond to the value calculated from free energy data.

In a recent paper (1) a unified mechanism of passivity and inhibition based on the behavior of local elements on metal surfaces was outlined. In that paper mention was made of earlier work (2) on the behavior of local cells when an inhibitor, potassium chromate, was added to the corroding solution. In the earlier paper (2) the data on local cell behavior were presented in such a compact form that the connection between the two papers may not be obvious. For this reason it was believed desirable to replot the data in the form of local cell polarization diagrams to simplify the interpretation of the results. The polarization diagrams resulting from a replot of the data in Fig. 1 of the earlier paper (2) are given in Fig. 1 and 2.

Note that the addition of potassium chromate to a 10 per cent sodium chloride solution caused several changes in the characteristics of local corrosion cells on an aluminum specimen. Chromate addition increased the polarization of the local anodes but also decreased the polarization of the local cathodes. This latter effect is to be expected because of the oxidizing properties of the chromate ion. Since the increase in anodic polarization was greater than the decrease in cathodic polarization, the corrosion current was reduced. In other words, the chromate functions as an inhibitor because it increases anodic polarization and in spite of the fact that it decreases cathodic polarization.

It will also be noted that the apparent single potential (the potential of the short-circuited local cells) of the entire specimen moves in a cathodic direction as the chromate content is increased. It is obvious, however, that if the chromate had not depolarized the local cathode, this movement of potential in a cathodic direction would not have been as pronounced (see I_2 in Fig. 2).

Movement of the apparent single potential in a cathodic direction is not of itself an indication that inhibition (or passivity) is occurring. Such a movement can be caused by either depolarization of the local cathodes, or polarization of the local anodes. The former effect, *if it is the only change in local cell behavior*, will result in an increase in corrosion rate. This is illustrated in some earlier work by the

[1] Manuscript received November 16, 1949. This paper prepared for delivery before the Chicago Meeting, October 12 to 15, 1949.

authors (3) with stainless steel. Here it was found that in sodium chloride solution the corrosion reaction of stainless steel is under mixed control; that is, appreciable polarization of both the local anodes and of the local cathodes occurs. If ferric chloride is added to the solution, depolarization of the cathodes occurs thus permitting a greater corrosion current to flow. The apparent single potential of the specimen, however, moves in a cathodic direction. For example, when the anode is limited to one pit, the apparent single potential of the entire sample is about −0.33 volt in sodium chloride solution. If 0.84 gram of ferric chloride is added per liter of sodium chloride solution, the apparent single potential moves in a cathodic direction to −0.235 volt although the corrosion current increases about 10 times (from 0.016 milliampere to 0.16 milliampere). In this case if an attempt had been made to evaluate the effect of ferric chloride by single potential measurements alone (as has been done by some workers), ferric chloride would be classed as an inhibitor, since it caused the apparent single potential to move in a cathodic direction. Actually, of course, ferric chloride greatly stimulates corrosion.

From the two examples described above, it is evident that, in order to interpret the meaning of a shift in the apparent single potential, it is necessary to know the nature of the changes in behavior of the polarization characteristics of the local anodes and cathodes.

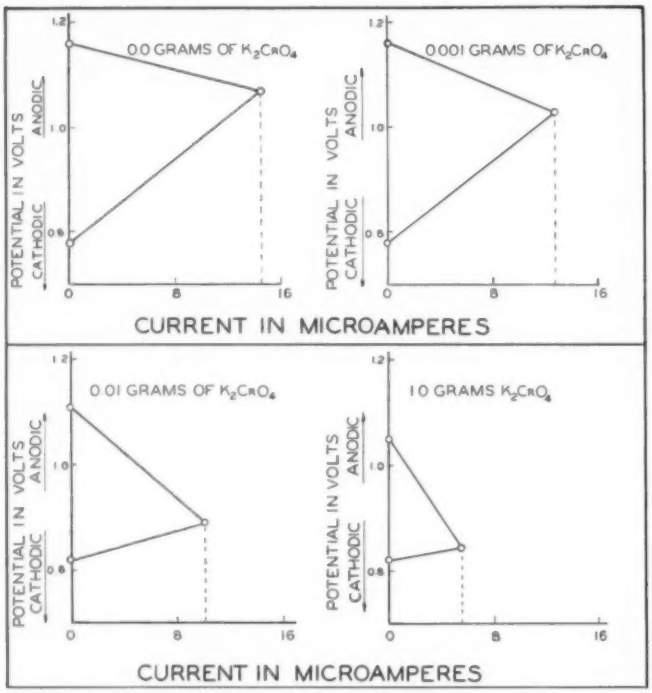

FIG. 1. Effect of concentrations of chromate on local cells on aluminum in 10% NaCl solution.

Suggestions have been made for evaluating the effect of inhibitors by measuring the anodic and cathodic polarization curves in solution free from or containing the inhibitors. In these cases, polarization was achieved by applying potentials from an external source. The anodic or cathodic polarization was then measured in the same manner. Although, superficially, this might seem to be similar to measuring the polarizations of the local anodes and cathodes on the metal surface, closer examination shows that it is quite different. In fact, results of such polarization measurements using applied potentials do not necessarily bear any simple relationship to results of polarization measurements on the local cells.

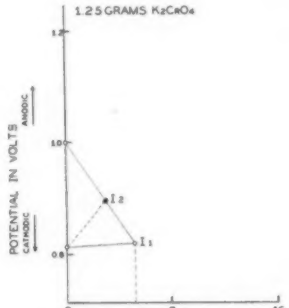

FIG. 2. Effect of concentration of chromate on local cells on aluminum in 10% NaCl solution.

In the local cell diagrams given in Fig. 1 and 2, the polarization curves for the local anodes and local cathodes are shown as straight lines. This is sometimes approximately correct, especially if the potentials of the local anodes differ only slightly from those of the local cathodes. However, in the general case, it cannot be assumed in advance that either anodic or cathodic polarization curves will be straight lines (4). Yet some workers have apparently made this assumption and have used methods of evaluating the mechanism of inhibitor action based on determination of the shape of anodic and cathodic polarization curves or the extent of anodic or cathodic polarization when the entire specimen was polarized by current from an outside source. That is, they have neglected the polarization characteristics of the

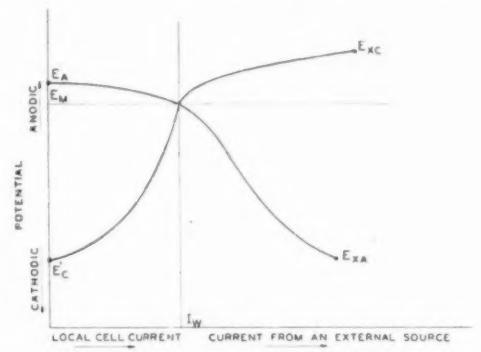

FIG. 3. Comparison between local cell polarization characteristics and polarization characteristics of specimen when current from an external source is applied.

local cells. Measurements made by polarizing the entire specimen with current from an external source may be very misleading as is indicated in the following discussion.

Let us assume that the shape of the local cell and "applied current" polarization curves are as illustrated in Fig. 3. If the local cell polarization curves are known, it is evident that the corrosion reaction is under cathodic control; i.e., cathodic polarization is much more pronounced than anodic polarization. If, however, the applied current method of determining polarization curves is used, then it will be concluded that anodic polarization is mainly controlling the corrosion reaction. This is, of course, incorrect.

In spite of the obvious likelihood of obtaining misleading results, the applied current method of measuring polarization has been much more widely used than has any method for measuring the local cell polarization curves. Probably the main reason for this is that it is difficult to measure local cell polarization curves. Curves of this type can only be obtained by direct measurement if it is possible to separate the local anodes and cathodes electrically. Direct measurements of this type have been reported by Evans and Hoar, Brown and Mears, and a few others. It is apparent, however, that the majority of corrosion processes cannot be studied in this manner since it is generally not possible to separate the local anodes and cathodes electrically.

Indirect Methods of Measuring Local Cell Polarization Curves

At least two indirect methods of measuring the polarization curves of the local anodes and cathodes are known. These are the "potential break" method and the "equivalent corrosion current" method. In the potential break method a cathodic and an anodic polarization curve of the specimen are run, using current from an external source. If the areas of the

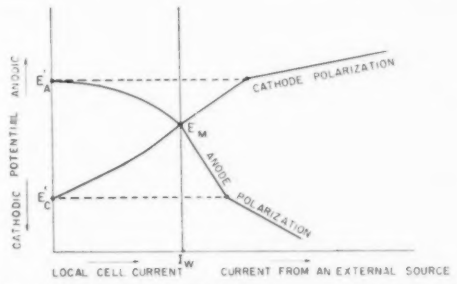

FIG. 4. Potential break method of studying characteristics of local cells.

local anodes and cathodes on the surface of the specimen are approximately of the same size and if some other conditions are met, curves of the type shown in Fig. 4 are frequently obtained. That is, changes in the slopes of the applied current polarization curves occur at potentials equal to the open circuit potentials of the local anodes and the local cathodes, respectively. If, now, the corrosion rate of the specimen, when no current is applied, is measured and the current equivalent to this rate is calculated it becomes possible to place points E'_A, E'_C and E_M on the diagram of Fig. 4 and thus to obtain the approximate average slopes of the polarization curves of the local anodes and cathodes.

The equivalent corrosion current method is similar but may have a somewhat broader applicability than the potential break method since it can be used even when sharply defined changes in slopes of the applied current polarization curves are not obtained. The basis of the equivalent corrosion method is the fact that the corrosion (weight loss) of the metal is directly proportional to the product of current leaving the anodic area and the time this current flows (time of exposure). This may

be expressed mathematically,

$$W = kI_w\theta; \qquad I_w = \frac{W}{k\theta}$$

where

W = weight loss.
θ = time of exposure.
k = proportionality constant which is dependent on the anodic reactions.
I_w = the corrosion current corresponding to the weight loss.

When the weight loss occurs only on the anodic areas, the anodic current I_A is equal to the current I_w. If several specimens of a metal are exposed for the same period of time in a solution with applied currents of various magnitudes in the range from zero to several finite values so that the specimen is cathodic with respect to the applied current, the weight loss of the specimen will depend upon the magnitude of the applied current. If the potentials of the specimens are measured against the same reference electrode, graphs can be made, one of external cathodic current I_{XC} versus the current I_w (equals I_A, the local anode current) and the other I_{XC} versus E_{XC}, the measured potential at various values of applied current (Fig. 5). When the applied current is cathodic, $I_w = I_A$, then it follows that E_{XC} also corresponds to the polarized potentials, E_A, of the local anodes. Hence a graph of E_A and I_A is the polarization curve of the local anodes. Repeating the experiment with another group of similar specimens with the current applied in such a direction that the specimens are anodic, another weight loss curve can be obtained; that is, the applied anodic current, I_{XA}, is plotted against I_w, the current calculated from the weight loss (Fig. 6). In addition, a graph of I_{XA} versus E_{XA}, the potential of the metal at various values of applied anodic current can be drawn. By virtue of the fact that when the specimens are anodic, $I_w = I_{XA} + I_C$, a graph can be prepared of I_{XA} versus $I_w - I_{XA}$ which equals I_C. Since, E_{XA}, the measured potentials of the metal indicates also the polarized potentials of the local cathodes, a graph of E_{XA} (equals E_C) versus $I_w - I_{XA}$ which equals the local cathodic current, I_C, is the polarization curve of the local cathodes. By combining this curve with that of the curve obtained as described previously, the anodic polarization of the local anodes, the polarization diagram of the local cells of the electrode is completed (Fig. 7).

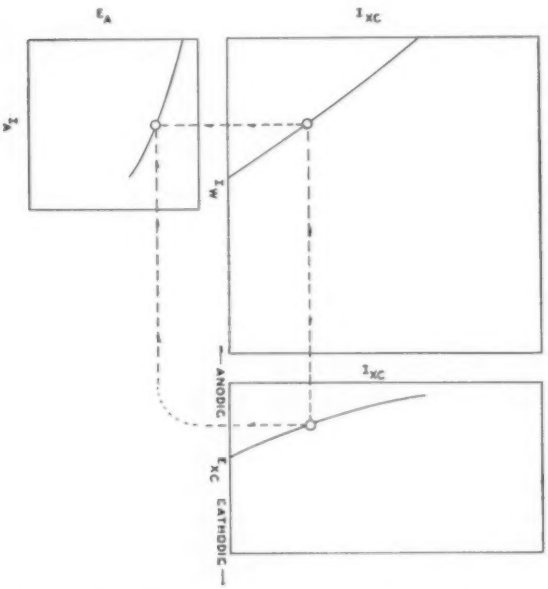

FIG. 5. Equivalent corrosion current method–method of obtaining polarization curve of local anode.

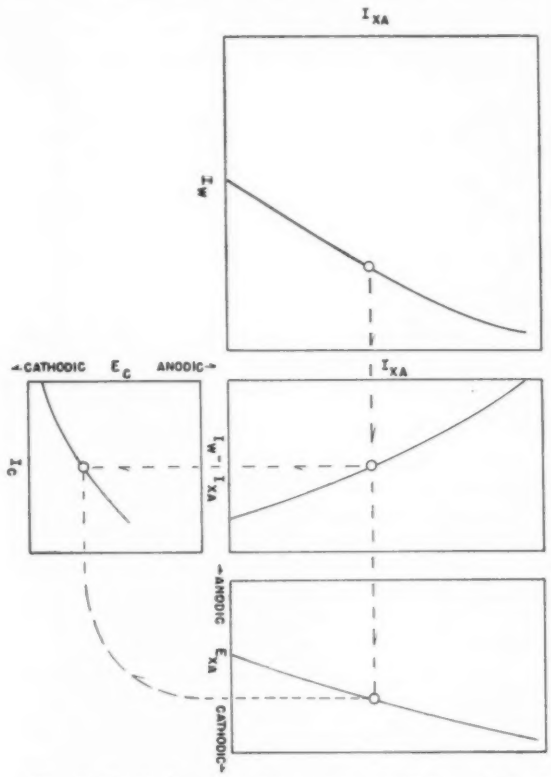

FIG. 6. Equivalent corrosion current method–method of obtaining polarization curve of local cathode.

From local cell polarization curves established by either of the methods just described the type of control, anodic, cathodic, or mixed, can be determined. The effects of inhibitors or accelerators on the behavior of the local cells can be studied in this manner.

By the use of these methods, information on the behavior of local cells can be studied under corrosion conditions where it is not possible to separate the local anodes and cathodes. Nevertheless, both methods have definite limitations so that additional methods of studying local cell behavior are desirable.

For example, both methods will probably fail if the areas of the local anodes and cathodes change as the specimen is polarized either anodically or cathodically with current from an outside source. Also, in the preceding discussions and in the polarization diagrams, all anodic areas or all cathodic areas on any one specimen are assumed to have the same open circuit potential. If several different anodes (or cathodes) are present which have different open circuit potentials, the complications may become so great that interpretation will be difficult. In addition, if the fundamental oxidation and reduction reactions change, the methods may give erroneous results. Thus, while the use of such methods may extend the variety of conditions under which local cell polarization curves can be studied, they are not applicable to all corrosion processes.

Comparison of Measured Open Circuit Potentials and Potentials Calculated from Thermodynamic Equations

It will be observed that, in many cases, the measured open circuit potentials of neither the local anodes nor the local cathodes of a metal specimen exposed to an aqueous solution correspond to values that can be calculated from thermodynamic equations of electrode potentials. For example, the equation for the thermodynamic electrode potential at 25° C of aluminum on the $\frac{N}{10}$ calomel scale is

$$e_{Al} = -2.01 + 0.0197 \log (Al^{+++})$$

where Al^{+++} is the activity of the aluminum ion. In an essentially neutral solution, such as a 10 per cent by weight solution of sodium chloride, the value e_{Al} will be more negative (more anodic) than -2.01 because the solubility of Al^{+++} ions is very low. Thus, in the absence of any local cell action, the potential of an aluminum specimen in a 10 per cent sodium chloride solution should be substantially lower than -2.01 volts on the $\frac{N}{10}$ calomel scale. Actual measurements of the potential of even the anodic areas on an aluminum specimen exposed to such a solution do not exceed about -1.1 volts (see Fig. 1). This disagreement is caused by irreversible effects resulting from local cell action within the apparent anodic area. In some cases the nature of the local cell action is such as to permit agreement between measured potentials and values calculated from thermodynamic equations. It has been generally overlooked that local cell action is occurring even in cases where agreement between the measured and the calculated values was obtained.

Even in the most simplified case, it may be considered in the actual measurement of the potential of a metal in a solution that two reactions are involved; one an anodic reaction, that is an oxidation reaction, and a cathodic reaction, that is a reduction reaction. In the general case there are several oxidation and reduction reactions. Considering the simplified case of a metal electrode in an aqueous solution completely free of oxygen the anodic (oxidation) reaction would be

$$M \rightleftharpoons M^{+} + 2\theta \qquad \text{(I)}$$

and the cathodic (reduction) reaction would be

$$2H^{+} + 2\theta \rightleftharpoons H_2 \qquad \text{(II)}$$

Usually all electrode reactions are written as oxidation reactions in order to codify thermodynamic data. From the thermodynamic data, the electrode potential of a given electrode reaction can be calculated by means of equations derived from thermodynamic considerations. Only with specific solutions and conditions will the measured potential correspond to that calculated from thermodynamic data. The thermodynamic equation for reaction (I) is

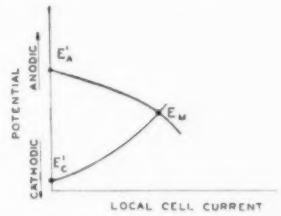

FIG. 7. Polarization diagram of local cells obtained from equivalent current method.

$$e_M = E_M + \frac{RT}{NQ} \ln (M^{++}) \qquad \text{(III)}$$

where

e_M = the calculated potential of the electrode (usually referred to as the reversible or equilibrium potential of the electrode) against some reference electrode.
E_M = the electrode potential when (M^{++}) has a value of unity.
R = gas constant.
T = temperature in °K.
(M^{++}) = activity of the metallic ions in the solution in moles per thousand grams of solvent.

In dilute solutions the activity (M^{++}) approaches the concentration of the metallic ions $C_{M^{++}}$. In further discussions the activities of the ions will be considered as equal to their concentrations. The thermodynamic equation for the potential of the hydrogen-hydrogen ion electrode at 25°C (reaction 2) on the saturated calomel scale is

$$e_{H_2} = -0.2458 + 0.059 \log \frac{C_{H^+}}{(pH_2)^{1/2}} \quad \text{(IV)}$$

Another possible reaction besides reaction (I) and (IV) is

$$2H_2O = O_2 + 4H^+ + 4\,\theta \quad \text{(V)}$$

and the thermodynamic electrode potential at 25°C on the saturated calomel scale for such a reaction is given by the equation

$$e_{O_2} = 0.9812 + 0.059 \log (C_{H^+})\,(P_{O_2})^{1/4} \quad \text{(VI)}$$

Because McAulay and Spooner (5) have measured the potential of cadmium in solutions containing various concentrations of cadmium chloride, the reaction

$$Cd = Cd^{++} + 2\,\theta \quad \text{(Ia)}$$

will be used to study the conditions which permit the measured potentials to correspond to those calculated from the thermodynamic equations. The thermodynamic potential on the saturated calomel scale of the cadmium electrode may be calculated from the thermodynamic equation of potential for reaction (Ia):

$$e_{Cd^{++}} = -0.6478 + 0.0295 \log (Cd^{++}) \quad \text{(VII)}$$

The potential of the cadmium-cadmium ion electrode at a cadmium ion concentration of 10^{-3} molal is -0.7363 volt. If the same solution is essentially free of dissolved gaseous oxygen and at a pH of 7, the potential calculated from the thermodynamic equation at a pressure of one atmosphere of hydrogen is -0.6588 volt, that is, 0.0775 volt cathodic to the potential developed by the cadmium-cadmium ion electrode. Obviously these two potentials cannot exist at the same electrode without some adjustment of either the hydrogen-hydrogen ion reaction (cathodic reaction) or the cadmium-cadmium ion reaction (anodic reaction). Since the measured potential corresponds very closely to the calculated value for the reaction,

$$Cd \rightleftharpoons Cd^{++}\,(10^{-3}\ \text{mole}) + 2\,\theta$$

it means that the potential for the reaction

$$H^+ + 1\,\theta = \tfrac{1}{2}H_2$$

on cadmium must be altered to that of the cadmium-cadmium ion thermodynamic potential[2]. Under these conditions the polarization is such that the measured potential corresponds to that calculated from thermodynamics or the so-called "reversible" or "equilibrium" potential.

For those metals and conditions where e_M of equation (III) is more anodic than e_{H_2} of equation (IV), the measured potential can only correspond to the calculated potential if there is no polarization of the anodic (metal-metal ion) reaction and complete polarization of the cathodic (hydrogen-hydrogen ion) reaction. In other words, such correspondence of measured and calculated values can only occur under conditions of complete cathodic control. If, in absence of oxygen, the measured potential of a metal-metal ion electrode is more cathodic than the value calculated from thermodynamics for a metal-metal ion electrode and more anodic than that calculated for the hydrogen-hydrogen ion electrode, then the metal-metal ion reaction is polarized as well as the hydrogen-hydrogen ion reaction. Hence the local cells are under mixed control. If the measured potential of the metal-metal ion electrode is almost equal to that of the potential calculated from thermodynamic data for the hydrogen-hydrogen ion electrode then only the metal-metal ion reaction is polarized and the local cells are under anodic control. These latter two conditions are frequently approached by some of the more anodic metals in aqueous solutions.

If dissolved oxygen is present in the electrolyte, the potentials of metals are usually more cathodic than if oxygen is absent. If the local cells function so that the anodic reaction is not polarized and the hydrogen-hydrogen ion reaction is highly polarized, so that the measured potential corresponds to the value calculated from thermodynamics for the *correct* metal ion activity, the reasons for the potential moving in a cathodic direction can be explained. With oxygen present the cathodic reaction (reaction VII)

$$\tfrac{1}{2}O_2 + 2H^+ + 2e \rightleftharpoons H_2O \quad \text{(VIII)}$$

can occur only if the anodic reaction

$$Cd \rightleftharpoons Cd^{++} + 2e$$

takes place. Combining these two reactions results in the overall reaction

$$Cd + \tfrac{1}{2}O_2 + 2_{H^+} \rightleftharpoons Cd^{++} + H_2O \quad \text{(IX)}$$

The equilibrium constant shows that this reaction can proceed to the right to such an extent that

[2] The potential of cadmium in a 10^{-3} molar solution of $CdCl_2$ at 18° C was found (McAulay and Spooner) to be -0.747 volt. At 25° C the value calculated from thermodynamics is -0.7363 volt.

essentially all the oxygen is consumed. The concentration of Cd^{++} ion which results from the above reaction is limited only by the concentration of the oxygen and the pH of the electrolyte.

Again using cadmium to illustrate the effect of oxygen causing the potential to become more cathodic, consider cadmium immersed in a dilute electrolyte at 25°C free of cadmium ions at a pH of 7 and saturated with oxygen from the contacting air. The concentration of oxygen would be about 2.6×10^{-4} moles per liter. Reaction of this oxygen according to equation (IX) would result in the formation of 5.2×10^{-4} moles of Cd^{++} ion providing no oxygen was allowed to diffuse into the system. Using equation (VII), the thermodynamic potential is calculated to be -0.7448 volt. Obviously unless cadmium ion is added in concentrations of the order of 10^{-4} moles or greater, the potential will not be altered. Fig. 8 shows the effect of added cadmium ion concentrations and of initial oxygen concentrations on the potential of the cadmium electrode. Consequently the results of McAulay and Spooner are explained on a thermodynamic basis if the hydrogen-hydrogen reduction reaction is highly polarized. It would appear that the so-called "rigidly air-free solutions" of McAulay and Spooner contained about 6.0×10^{-6} moles of oxygen per liter. If an excess of oxygen can be maintained in the solution, the oxygen and metal reactions can both be polarized with the result that the measured potential can be between the thermodynamic potential for each reaction.

The above discussion has been concerned with the chemical and electrochemical factors (that is, true polarization) which may cause the measured potential to differ from the thermodynamic potential. By true polarization is meant the back emf which may be created at an electrode surface as the result of current flow. The passage of current may also introduce factors which will affect the measured potential. Assume a metal covered with a film of oxide or hydroxide which has a high ohmic resistance to the passage of current, but the anodic reaction

$$M \rightleftharpoons M^{++} + 2e$$

can proceed without producing any back emf. As a result, the passage of current will produce an IR drop across the film. This IR drop will be included in the potential between the reference electrode and metal electrode. The potential measurement will be more cathodic than the true potential (the thermodynamic potential) of the electrode if the current is leaving the metal and entering the solution and more anodic if the current is entering the metal from the solution. Furthermore, IR drops in the solution between the electrode and the reference electrode will also be included in the measurements of the potential. Therefore, the potential of a metal in a solution in which local cells are functioning, against a reference electrode can, in general, be expressed by two equations, one for the anodic element and another for the cathodic element. These equations are:

$$E_X = e_{A\,R} - E_a^1 - IR_a - Ir_{as} \qquad (X)$$

and

$$E_X = e_{C\,R} + E_c^1 + IR_c + Ir_{cs} \qquad (XI)$$

where

E_X = measured potential between the metal electrode and the reference electrode.

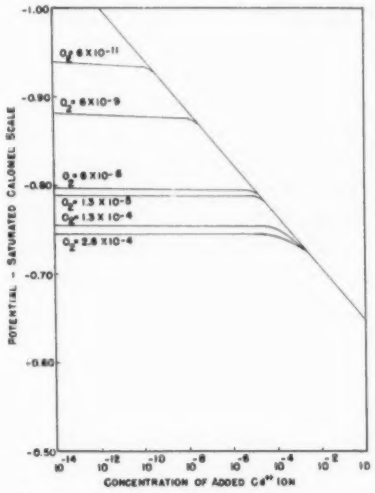

FIG. 8. Effect of added cadmium ion concentration and of initial oxygen concentration on the potential of a cadmium electrode.

$e_{A\,R}$ = potential of metal-metal ion electrode calculated from the thermodynamic equation

$$e_{A\,R} = E_M + \frac{RT}{NF} \ln (M^{++}).$$

E_a^1 = back emf produced by the passage of the local action current from the anode areas to the solution which is a function of the current I and the area of the anode element.

IR_a = IR drop produced by the passage of local action current through the films on the surface of the anode areas. Note that this voltage drop produces an I^2R loss in contrast to the voltage drop E_a^1.

Ir_{as} = IR drop in the solution between the reference electrode and the anode areas on the metal electrode.

e_{CR} = potential developed by the cathode reaction, for example $H^+ \rightleftharpoons \frac{1}{2}H_2 + \theta$, calculated from the thermodynamic equation. This equation for the hydrogen-hydrogen ion reaction is

$$e_{CR} = E_{H_2} + \frac{RT}{F} \ln \frac{H^+}{pH_2^{\frac{1}{2}}}$$

E_c^1 = back emf produced by the passage of the local action current from the solution to the cathode areas which is a function of the current I and the area of the cathode element.

IR_c = IR drop produced by the passage of the local action current through the films on the surface of the cathode areas.

Ir_{cs} = IR drop in the solution between the reference electrode and the cathode areas on the metal electrode. Ir_{cs} does not, in general, equal Ir_{as}.

Obviously, equation (X) equals equation (XI).

It can be seen that many factors can be involved in the measurement of a single electrode potential. Indeed, the measured potential of a metal in a solution of its ions can only be equal to the thermodynamic potential if

$$e_{AR} = e_{CR} + E_c^1 + IR_c \text{ or } e_{AR} = e_{CR}.$$

The latter case would be most rare because the concentration of ions and compounds involved in the cathodic reaction would have to be such as to adjust the cathode potential to that of anode potential without any back emf or IR drop.

Conclusions

It is concluded that the inhibiting action of sodium chromate on localized corrosion of aluminum exposed to a sodium chloride solution is mainly the result of polarization of the local anodes. Sodium chromate would be an even more effective inhibitor if it did not also depolarize the local cathodes. Additions of ferric chloride to a sodium chloride solution stimulate the localized corrosion of 18-8 stainless steel because ferric chloride acts as a cathodic depolarizer and has little effect on the polarization characteristics of the local anodes. In both of the above examples, the apparent single potential of the specimen moves in a cathodic direction. Thus, measurements of changes in apparent single potentials are of little value by themselves in studying the mechanism of inhibitor action (or passivity).

Similarly, polarization curves obtained by the use of currents from an external source do not directly indicate the mechanism of inhibitor action. Two indirect methods of studying the effects of changing environment on local cell behavior are described. Both of these methods have severe limitations so that an additional method or methods are desirable.

It is indicated that local cell reactions are probably occurring even in those cases where measured single potential values agree with those calculated from thermodynamic data. Such correspondence between measured single potentials and those calculated from thermodynamic data will only be obtained when there is a specific type of local cell action.

Any discussion of this paper will appear in a Discussion Section, to be published in the December 1950 issue of the JOURNAL.

REFERENCES

1. R. B. MEARS, *J. (and Trans.) Electrochem. Soc.*, **95**, 1 (1949).
2. G. G. ELDREDGE AND R. B. MEARS, *Ind. Eng. Chem.*, **37**, 738 (1945).
3. R. H. BROWN AND R. B. MEARS, *Trans. Faraday Soc.*, **35**, 469 (1939).
4. See, for example, experimentally determined polarization curves in the following papers:
   R. H. BROWN AND R. B. MEARS, *Trans. Faraday Soc.*, **35**, 470 (1939); *Trans. Electrochem. Soc.*, **74**, 509 (1938).
   L. J. BENSON, R. H. BROWN, AND R. B. MEARS, *Trans. Electrochem. Soc.*, **76**, 264 (1939).
5. A. L. MCAULAY AND E. C. R. SPOONER, *Proc. Roy. Soc. London*, **138A**, 494 (1932).

Barium-Magnesium Silicate Phosphors[1]

KEITH H. BUTLER AND JAMES G. CASSANOS

Sylvania Electric Products, Inc., Salem, Massachusetts

ABSTRACT

The complex four-component system, containing barium oxide, magnesium oxide, lead oxide, and silicon dioxide, has been explored and several new phosphors were discovered which emit blue-white or blue-green light when excited by 2537 Å radiation. One of two definite crystal structures is found in the best phosphors. The first of these is a modified barium mesotrisilicate which emits light much like magnesium tungstate. The second is a complex silicate of variable composition and this fluoresces blue-green. Both compounds were previously found in barium-lead silicate phosphors, and the introduction of magnesium mainly improves the efficiency of the fluorescence.

Powder patterns obtained by x-ray diffraction indicate that at least four other new complex silicates may exist, but their composition has not been established and the powder patterns themselves are somewhat uncertain because mixtures of two or more components were almost invariably present.

INTRODUCTION

The preparation and properties of some lead-activated barium silicate phosphors were described in a previous paper (1). These phosphors can be efficiently excited by 2537 Å radiation and emit blue or blue-green light. It was found that the color and the efficiency were dependent on the ratio of silicic acid to barium and lead. The phosphors were classified in three groups: (*a*) $BaO \cdot SiO_2$ phosphors (*b*) $2BaO \cdot 3SiO_2$ phosphors, and (*c*) mixed phosphors. These three classes contain characteristically large amounts of lead, so that lead in addition to being the activator is also a modifier of fluorescence, varying the color. Clapp and Ginther (2) have described a $BaO \cdot 2SiO_2$ phosphor which emits ultraviolet light. This represents a fourth group.

The present paper describes lead-activated barium silicate phosphors in which the color is varied by introducing magnesium as a modifier. The system is even more complex than the barium silicate system because of the introduction of the fourth component and only a general outline of the properties can be given.

CRYSTAL STRUCTURE OF THE PHOSPHORS

In the previous paper on barium silicates, the x-ray powder patterns of four compounds were listed. These were identified as (*a*) $BaO \cdot SiO_2$, (*b*) $2BaO \cdot 3SiO_2$, (*c*) $BaO \cdot 2SiO_2$, and (*d*) pattern "X." It was also indicated that a fifth compound with a high lead content might exist.

Further work on this system has established that pattern "X" is obtained over a considerable range of compositions with the lead oxide content varying from 0.1 to 0.4 moles per mole of barium oxide and the net silicic acid[2] content varying from 1.0 to 1.2 moles per mole of barium oxide. We may tentatively give this compound the formula $3BaO \cdot PbO \cdot 4SiO_2$. The second compound mentioned, which can be identified as pattern "Z," appears over an even wider range of compositions with lead contents of 0.4 to at least 1.2 moles PbO per mole of BaO and silicic acid content of 0.9 to 1.6 net moles[2] per mole of BaO. The strongest characteristic fluorescence was obtained with a composition approximating the formula $BaO \cdot PbO \cdot 2SiO_2$ and this formula can be tentatively ascribed to the compound giving pattern "Z."

These same patterns "X" and "Z" appear frequently in the barium-magnesium-lead silicate phosphors as well as four new patterns definitely different from the barium silicates or the magnesium silicates. The introduction of magnesium appears to change the allowable range of compositions for compound "Z" so that it appears with lower lead content and lower SiO_2 content than for the system without magnesium. The powder diffraction data for these new patterns are listed in Table I, as tentatively identified.

There appears to be some association of two of these new compounds since compound "Z" is frequently accompanied by pattern "A" with varying intensity as shown in Table II.

Patterns B, C, D, were obtained only for a few special compositions as shown in Table III.

It is possible that other unexplored compositions will also show these patterns but such further exploration has not been completed at the present time.

[1] Manuscripts received October 28, 1949. This paper prepared for delivery before the Cleveland Meeting, April 19 to 22, 1950.

[2] "Net SiO_2" is the SiO_2 per mole of BaO after allowing one mole SiO_2 for each mole of PbO.

Experimental Methods

The raw materials used in preparation of the phosphors were the highest quality reagent grade chemicals. They included barium carbonate, silicic acid, lead carbonate, and basic magnesium carbonate. They were assayed by chemical analysis before calculating the raw material blend, which was prepared by grinding in water in a porcelain ball mill with flint pebbles. The thick, ball-milled slurry was filtered and dried, after which it was either crushed or hammer-milled. The powders were fired in open silica or porcelain crucibles in a globar-heated furnace for 4 hours. The air-cooled powders were mortar-ground and then refired for 4 hours. The temperature for the second firing was generally 760°C whereas that employed for the first firing depended on the composition.

Testing methods were identical with those previously employed (1) and outputs are relative to a a calcium-lead tungstate standard.

TABLE I. *X-ray powder diffraction data**

Compound "Z"		Pattern "A"		Pattern "B"		Pattern "D"	
I	*d*	*I*	*d*	*I*	*d*	*I*	*d*
W	5.27	W+	6.3	W+	5.4	W	4.6
W	3.62	W+	4.6	W	4.07	VVW	4.06
W+	3.40	W	3.90	W	3.93	VVW	3.87
M+	3.33	M+	3.23	W+	3.64	M	3.22
W+	2.97	M	3.16	W+	3.25	VW	3.13
W	2.75	VVW	2.91	S	3.02	M	3.00
VW	2.56	VVW	2.86	W	2.69	VW	2.85
W	2.20	W+	2.50	W	2.58	W−	2.76
W+	2.14	W−	2.45	VW	2.43	W−	2.68
VW	2.09	VVW	2.36	W	2.32	W−	2.56
W+	2.05	VVW	2.31	W	2.25	W−	2.49
W	1.88	W+	2.26	M	2.17	VVW	2.36
W	1.82	VVW	2.01	W−	2.04	VW	2.31
W+	1.78	VW	1.97	W	1.98	W	2.26
VW	1.71	W	1.94	W	1.92	VW	2.19
W+	1.68	VVW	1.85	M	1.86	W	2.15
W	1.65	W	1.75	W	1.81	VW	2.09
W	1.63			VW	1.65	W	2.04
W+	1.51			W+	1.61	VVW	2.00
				W	1.60	W	1.94
				W	1.57	W+	1.85
				VVW	1.54	VW	1.80
				VVW	1.51	W−	1.78
				W+	1.46	VVW	1.75
				VVW	1.40	VW	1.71
				VW	1.36	W−	1.69
				VVW	1.35		
				W	1.33		
				VW	1.32		
				W	1.24		
				W−	1.22		
				W	1.20		

* These patterns are only tentatively identified as belonging to the compounds listed. In general, two or more components were present and increase or decrease of relative intensities was the main criterion for believing certain lines belonged to a definite compound. "A" and "C" are very similar and may result from modifications of the same compound, hence only pattern "A" is listed, since we had numerous examples of pattern "A" but only a few cases of pattern "C."

General Outline of Phosphor System

Method of Approach

The BaO-MgO-PbO-SiO_2 system was investigated in terms of three independent variables, namely, the ratio of barium to magnesium (Ba:Mg ratio), the amount of silicic acid ("net" moles SiO_2), and the amount of lead. The moles of lead oxide and net moles of silicic acid were expressed on the basis of one mole of barium oxide plus magnesium oxide.

TABLE II

Mole composition			Total SiO_2	Net SiO_2	Intensity	
BaO	MgO	PbO			"Z"	"A"
0.6	0.4	0.2	1.2	1.0	Strong	Medium
0.6	0.4	0.2	1.1	0.9	Very strong	Weak
0.6	0.4	0.2	1.0	0.8	" "	Very weak
0.6	0.4	0.3	1.3	1.0	" "	Weak
0.6	0.4	0.3	1.2	0.9	" "	Very, very weak
0.4	0.6	0.1	1.1	1.00	Medium	Medium
0.4	0.6	0.1	0.85	0.75	"	"
0.4	0.6	0.1	0.75	0.65	"	"
0.4	0.6	0.2	1.20	1.0	Medium	Medium
0.4	0.6	0.2	0.95	0.75	Strong	Weak
0.4	0.6	0.2	0.85	0.65	Strong	Weak
0.4	0.6	0.2	0.80	0.60	None	None
0.2	0.8	0.1	0.90	0.80	Medium	Medium
0.2	0.8	0.1	0.70	0.60	"	"
0.2	0.8	0.1	0.60	0.50	"	"

TABLE III

Mole composition			Total SiO_2	Net SiO_2	Pattern found
BaO	MgO	PbO			
0.6	0.4	0.2	0.80	0.60	B
0.6	0.4	0.3	0.80	0.50	B
0.6	0.4	0.2	0.70	0.50	B
0.6	0.4	0.1	0.70	0.60	C
0.6	0.4	0.1	0.60	0.50	C
0.6	0.4	0.2	0.60	0.40	C
0.4	0.6	0.2	0.80	0.60	D

The most thorough explorations were made of fields in which the lead and Ba:Mg ratios were varied and the net moles SiO_2 were kept constant at 1.50 moles, 1.30 moles, and 1.15 moles. A more limited survey was made of a similar field in which the net

SiO_2 was kept constant at 1.05 moles. Contour diagrams[3] for these fields are given in Fig. 1 to 7 inclusive, with the numbers on the various curves indicating relative brightness of the phosphors. Limited surveys (Fig. 8 to 11) were also made in which the Ba:Mg ratio was kept constant at 0.8:0.2, at 0.6:0.4, and at 0.4:0.6. Fig. 12 to 15 represent the effect of varying Ba:Mg ratio and silicic acid at constant lead.

The ranges covered on each of the variables were as follows, although the entire range of each variable was not explored for some of the fields:

Ba:Mg ratio—1.0:0.0 to 0.0:1.0
Net mole SiO_2 per mole (BaO + MgO)—2.05 to 0.4
Mole PbO per mole (BaO + MgO)—0.01 to 0.60

In the figures, "moles Ba" is an abbreviation for "moles BaO per 1.0 moles of barium oxide plus magnesium oxide," similarly "moles PbO" and "net SiO_2" refer to a basis of 1 mole (BaO + MgO).

Throughout the investigation of this system, it was necessary to fire samples at several different temperatures in order to find the one that gave the peak output. Quite often samples which were poor phosphors when fired at a given temperature improved considerably when fired at temperatures which were 25° to 50°C higher or lower. Unfortunately, it was not possible to determine the optimum firing temperature for each composition. The output curves on the contour diagrams, therefore, have been drawn as smooth curves whenever it was felt that peaks or depressions were caused by improper firing temperature.

Field of 1.50 Net SiO_2 (Fig. 1)

This field contains no phosphors that are an improvement over the corresponding barium lead silicates without magnesium. There is a gradual decrease in output in both the green and blue components as the barium is replaced by magnesium.

Field of 1.30 Net SiO_2 (Fig. 2 and 3)

This field has been explored more thoroughly than any of the others. The replacement of barium by magnesium results in improved phosphors and permits the use of less lead than is required by barium lead silicate. A peak is obtained in the contour diagram in the area around a Ba:Mg ratio of 0.8:0.2 and between 0.05 and 0.10 mole PbO. An interesting phosphor (type "I") in this area was studied further and is described in a later portion of this paper. The approximate composition is that of the point marked "A." At higher lead contents (0.2 to 0.6 mole) there is a broad area which is equal to, or better than, the corresponding barium lead silicate.

From the x-ray powder diffraction studies made on this field, it appears that in the area around Ba:Mg ratio of 0.8:0.2 and up to 0.20 mole of lead oxide the predominant crystal phase is the type of pattern obtained from barium mesotrisilicate phosphors, lead-activated, the addition of lead causing no apparent change in the spacings of the x-ray dia-

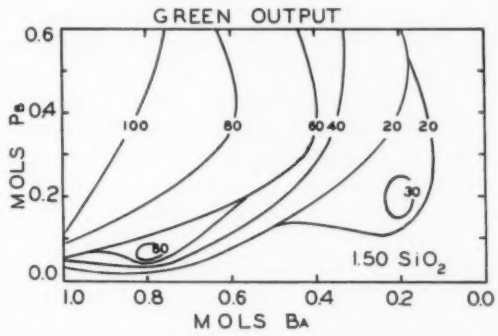

FIG. 1. Effect of lead content and Ba/Mg ratio on the green output of barium magnesium lead silicates with 1.50 net moles SiO_2.

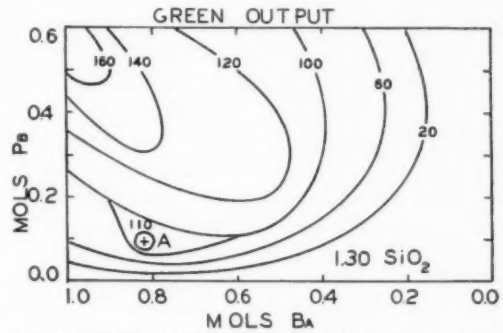

FIG. 2. Effect of lead content and Ba/Mg ratio on the green output of barium magnesium lead silicates with 1.30 net moles SiO_2.

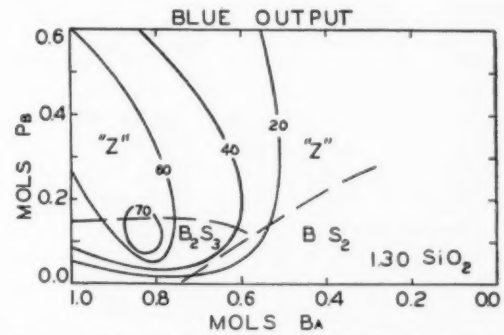

FIG. 3. Effect of lead content and Ba/Mg ratio on the blue output of barium magnesium lead silicates with 1.30 net moles SiO_2.

[3] Reference (1), page 273.

gram. The dashed lines in Fig. 3 show the areas in which particular patterns are predominant. B_2S_3 indicates $2BaO \cdot 3SiO_2$, whereas BS_2 indicates $BaO \cdot 2SiO_2$. The surprising thing is that the presence of 0.20 mole of magnesium silicate has very little effect on the spacings. Since the barium mesotrisilicate (1.50 net moles SiO_2 per mole BaO) is the barium compound formed, the following equation may serve to explain why the addition of 0.2 mole of magnesium oxide shifts the peak output of barium magnesium lead silicate (Ba:Mg-0.8:0.2) into the field of 1.30 net mole SiO_2.

$$0.8\ BaO + 0.2\ MgO + 1.3\ SiO_2 \rightarrow 0.4(2BaO \cdot 3SiO_2) + 0.1(2MgO \cdot SiO_2)$$

$$PbO + SiO_2 \rightarrow PbO \cdot SiO_2$$

These equations should not be interpreted as meaning that the three compounds exist independently. As x-ray data show, the resulting material is a single new compound and the interpretation is that the grouping of the Ba-O, Mg-O, and Pb-O polyhedra around the Si-O polyhedra cannot be identical with that occurring in the barium silicates, because of the different coordination of Ba, Mg, and Pb with oxygen. Thus, a reaction to form a compound in which barium and magnesium have the characteristic coordination and grouping occurring in barium mesotrisilicate and magnesium orthosilicate explains the mole composition required for peak output in the 1.30 net mole SiO_2 field with low lead. With this composition, the grouping of the lead-oxygen polyhedra around the Si-O tetrahedra apparently results in the same spatial relationships as are present in lead metasilicate ($PbO \cdot SiO_2$).

At higher lead content and a Ba:Mg ratio of 0.8:0.2, the predominant phase is compound "Z," discussed in a previous section. This compound, which also occurred with high lead in barium lead silicate, has a high green output and a relatively low blue output. At 0.2 mole PbO there is apparently a mixture of the two compounds, and some of the high blue output of the $2BaO \cdot 3SiO_2$ pattern is retained.

As magnesium replaces more of the barium, there is a tendency toward the formation of barium disilicate, especially if the powders are overfired. Samples which are fired normally and have high output show the compound "Z" pattern strongly at Ba:Mg-0.6:0.4. At low lead, the shift toward the barium disilicate may be explained if we assume a separate compound, though x-ray data to confirm this assumption are lacking.

$$0.4\ MgO + 0.2\ SiO_2 \rightarrow 0.2(2MgO \cdot SiO_2)$$

Thus the magnesium requires only 0.2 mole SiO_2 to complete its reaction leaving 1.1 mole SiO_2 to react with 0.6 mole BaO, almost enough to form $BaO \cdot 2SiO_2$. At higher lead content it is difficult to say what happens since the exact composition of compound "Z" is not known. The x-ray data show, however, that if firing conditions are right, the more efficient compound "Z" is formed in preference to barium disilicate. More data on the 1.30 net mole SiO_2 field are available in the discussion of Type I phosphor in a later section of this paper.

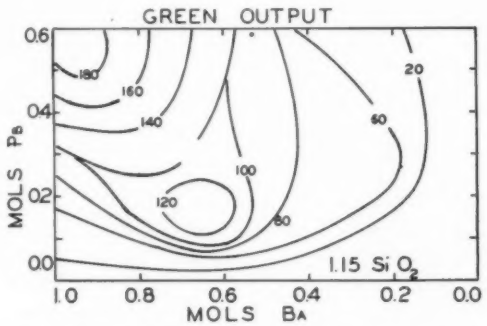

FIG. 4. Effect of lead content and Ba/Mg ratio on the green output of barium magnesium lead silicates with 1.15 net moles SiO_2.

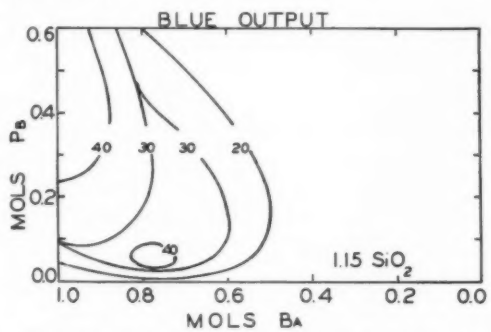

FIG. 5. Effect of lead content and Ba/Mg ratio on the blue output of barium magnesium lead silicates with 1.15 net moles SiO_2.

Field of 1.15 Net SiO_2 (Fig. 4 and 5)

In this field the substitution of magnesium for barium also produces more efficient phosphors at lower lead content than the corresponding barium lead silicate in the same field. Unfortunately, no x-ray data are yet available for this field, so statements on the probable compounds are in the realm of educated guesses.

It seems reasonable, however, to suppose that the compounds in the rectangle bounded by 0.3 and 0.6 mole Pb and Ba:Mg ratios of 1.0:0.0 and 0.6:0.4 have the same pattern, and that this pattern is the one due to compound "Z." The peak in the low lead area between 0.8 and 0.5 mole Ba may be explained

by the same reasoning as the peak in the 1.30 net mole SiO_2 field:

$$0.6\,BaO + 0.4\,MgO + 1.15\,SiO_2 \rightarrow 0.3(2BaO \cdot 3SiO_2) + 0.2\,(2MgO \cdot SiO_2) + 0.05\,SiO_2$$

In this field we may expect to find compound "X" or a modified barium mesotrisilicate.

Field of 1.05 Net SiO_2 (Fig. 6 and 7)

Only a limited survey was made of this field. The most promising point in the low lead area (BaO: MgO:PbO-0.7:0.3:0.1) was selected for the preparation of a large sample and designation as the Type

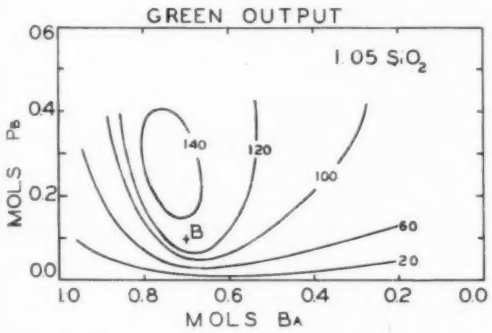

FIG. 6. Effect of lead content and Ba/Mg ratio on the green output of barium magnesium lead silicates with 1.05 net moles SiO_2.

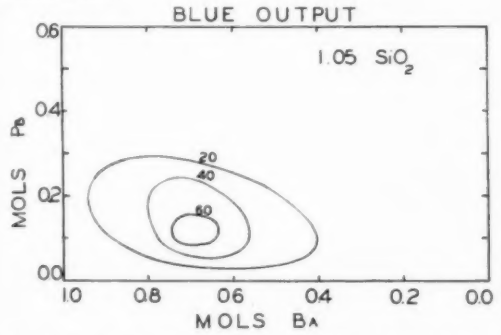

FIG. 7. Effect of lead content and Ba/Mg ratio on the blue output of barium magnesium lead silicates with 1.05 net moles SiO_2.

II phosphor. Point B shows the approximate composition of this type. Its characteristics are discussed in a later section.

In addition to the points covered in Fig. 6 and 7, four samples with very high lead and 1.05 net mole SiO_2 were prepared in an effort to set upper limits on the amount of lead. The results of these tests are given in Table IV, along with the values for barium lead silicate without magnesium.

Field of Ba:Mg-0.8:0.2

If the Ba:Mg ratio is kept constant at 0.8:0.2 and the lead and SiO_2 varied, a field is obtained which shows no new promising avenues of exploration, since for each value of lead there is a dropping off of output as the net moles of SiO_2 decrease and approach 1.0.

The net SiO_2 content at Ba:Mg ratio of 0.8:0.2 was carried up as high as 2.05 net SiO_2 in the range between 0.05 and 0.10 mole PbO. The green and blue emission of these points was negligible and the ultraviolet emission was only about 20 per cent of a standard blacklight phosphor. Since this area includes the phosphor developed by Clapp and Ginther, it may be assumed that magnesium will not improve the output of their phosphor.

Field of Ba:Mg-0.6:0.4 (Fig. 8 and 9)

In contrast to the previous field, it was found that when the Ba:Mg ratio of 0.6:0.4 was kept constant and the lead and silicic acid varied, the contour diagram showed that the output was still going up as the SiO_2 decreased and approached 1.0 net mole SiO_2. It was felt, therefore, that a peak might be obtained at less than 1.0 net mole SiO_2. It has been shown for

TABLE IV. *Characteristics of barium magnesium lead silicates with high lead content*

Ba:Mg ratio	Mole Pb*	Net mole SiO_2*	Output vs. % green	Std $CaWO_4$: Pb, % blue
1.0:0.0	1.20	1.05	157	26
0.8:0.2	1.20	1.05	90	16
0.6:0.4	1.20	1.05	63	12
0.4:0.6	1.20	1.05	37	6
0.2:0.8	1.20	1.05	11	1

* Per mole (Ba + Mg).

barium lead silicate that the compositions having less than 1.0 mole net SiO_2 per mole Ba were discolored. The presence of magnesium, however, apparently increases the solubility of lead in the matrix. At Ba:Mg-0.6:0.4 discoloration did not appear until the SiO_2 was reduced to 0.6 net mole.

Samples to establish the peaks in this field were prepared and from this field, phosphor Type III, BaO:MgO:PbO-0.6:0.4:0.2 at 0.9 net mole SiO_2, was selected as the most suitable for further tests (Point C on Fig. 8). This type phosphor is discussed in a subsequent section of the paper. The dashed lines on Fig. 9 block out roughly the regions in which barium disilicate, barium mesotrisilicate, and compounds "Z," "B," or "C" are predominant. Although there is general agreement between powder pattern and fluorescence, the valley of low output along the 1.2 mole SiO_2 line cannot be explained. The high blue peak is due to the presence of a modified barium mesotrisilicate whereas the powders with high green output are compound "Z," which must exist in two forms, one high in SiO_2 and the other low in SiO_2.

Field of Ba:Mg-0.4:0.6 (Fig. 10 and 11)

The most promising area of exploration at a Ba:Mg ratio of 0.4:0.6 also occurs below 1.0 net mole SiO_2 per mole (Ba + Mg). Although only a limited survey was made of this field, enough data were obtained to fix the peak at between 0.70 and

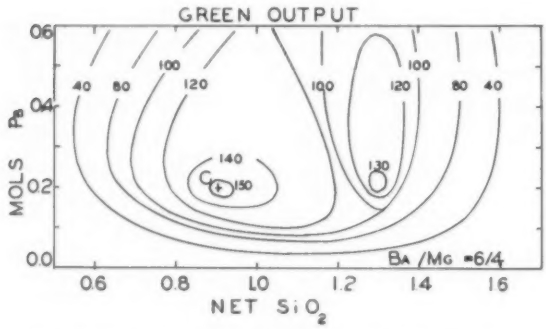

FIG. 8. Effect of lead content and net SiO_2 content on the green output of barium magnesium lead silicates containing 0.6 mole BaO to 0.4 mole MgO.

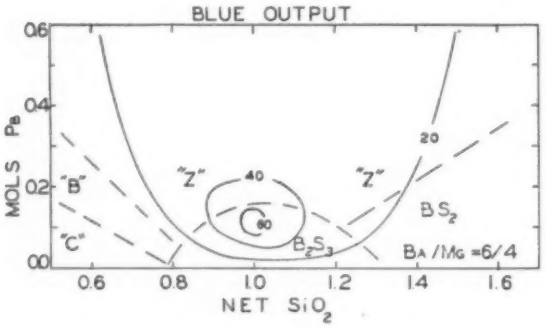

FIG. 9. Effect of lead content and net SiO_2 content on the blue output of barium magnesium lead silicates containing 0.6 mole BaO to 0.4 mole MgO.

0.75 net SiO_2. The composition at the peak could be explained as follows:

$$0.4\ BaO + 0.6\ MgO + 0.7\ SiO_2 \rightarrow 0.4\ (BaO \cdot SiO_2) + 0.3\ (2MgO \cdot SiO_2)$$

$$PbO + SiO_2 \rightarrow PbO \cdot SiO_2$$

The phosphor, Type IV, having the composition BaO:MgO:PbO-0.4:0.6:0.2 at 0.7 net mole SiO_2 was prepared and made into lamps (Point D on Fig. 10). This phosphor is discussed in a later section.

The predominant x-ray patterns are indicated in Fig. 11. The most striking feature is the appearance of Pattern A replacing roughly the field occupied by barium mesotrisilicate in Fig. 9. Pattern D replaces Pattern B. Here again there is fair agreement between x-ray patterns and fluorescence, but again there is evidence of two distinct modifications of compound "Z" with low and high silica contents.

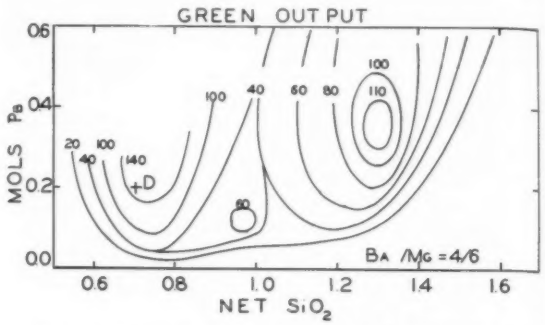

FIG. 10. Effect of lead content and net SiO_2 content on the green output of barium magnesium lead silicates containing 0.4 mole BaO to 0.6 mole MgO.

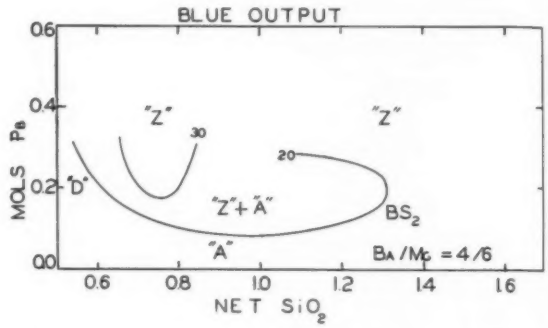

FIG. 11. Effect of lead content and net SiO_2 content on the blue output of barium magnesium lead silicates containing 0.4 mole BaO to 0.6 mole MgO.

TABLE V. *Barium magnesium lead silicate*
Ba:Mg = 0.2:0.8

Net mole SiO_2	Output vs. std $CaWO_4$:Pb			
	0.1 mole PbO		0.2 mole PbO	
	% green	% blue	% green	% blue
1.00	37	9	84	17
0.90	50	10	92	18
0.80	66	15	92	18
0.70	74	17	87	18
0.60	79	18	87	16
0.50	69	15	82	16

Field of Ba:Mg-0.2:0.8

Two sets of samples having a Ba:Mg ratio of 0.2:0.8 with varying amounts of SiO_2 were prepared and fired. The results of these tests are given in Table V.

At 0.1 mole PbO the output comes to a peak at

about 0.6 net mole SiO_2 indicating that the reaction might be as follows:

$$0.2\ BaO + 0.8\ MgO + 0.6\ SiO_2 \rightarrow 0.2\ (BaO \cdot SiO_2) + 0.4\ (2MgO \cdot SiO_2)$$

$$0.1\ PbO + 0.1\ SiO_2 \rightarrow 0.1\ PbO \cdot SiO_2$$

TABLE VI. *Barium magnesium silicate; effect of low barium* 0.2 mole PbO and 0.55 net mole SiO_2/mole (BaO + MgO)

Ba:Mg	Output vs. standard $CaWO_4$:Pb	
	% green	% blue
0.15:0.85	71	14
0.10:0.90	42	7
0.05:0.95	16	2
0.01:0.99	3	0
0.00:1.00	0	0

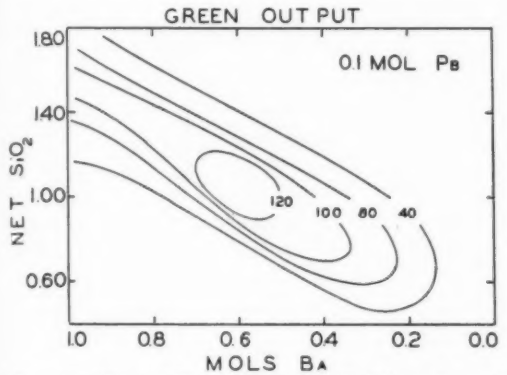

FIG. 12. Effect of SiO_2 content and Ba/Mg ratio on the green output of barium magnesium lead silicates containing 0.1 mole PbO.

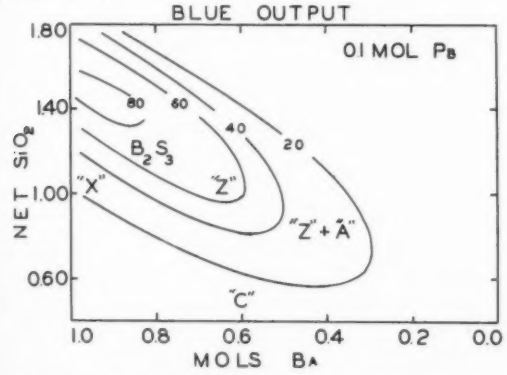

FIG. 13. Effect of SiO_2 content and Ba/Mg ratio on the blue output of barium magnesium lead silicates containing 0.1 mole PbO.

These samples show Patterns Z and A of about equal intensity. At 0.2 mole PbO the output remains about the same over a wide range, suggesting a pattern that is different from that at 0.1 mole PbO and x-ray data confirm this, only Pattern Z being found.

Compositions with Less than 0.2 Mole Ba per Mole (Ba + Mg) at 0.55 Net Mole SiO_2

One set of samples was run to determine the least amount of barium that could be used without complete extinction of fluorescence. For this particular series the net SiO_2 was held at 0.55 mole and the PbO at 0.2 mole per mole (BaO + MgO). Results are summarized in Table VI.

In addition to the above series, magnesium silicates, containing various amounts of silicic acid and lead, were prepared. None of these samples showed any fluorescence when exposed to 2537 Å radiation.

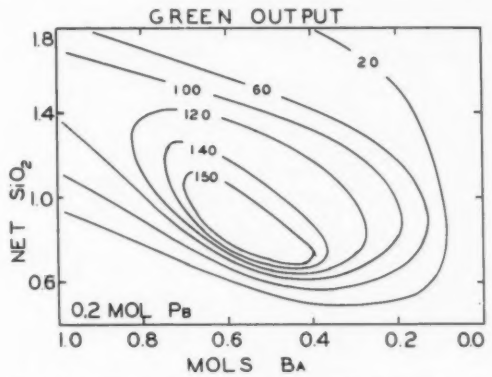

FIG. 14. Effect of SiO_2 content and Ba/Mg ratio on the green output of barium magnesium lead silicates containing 0.2 mole PbO.

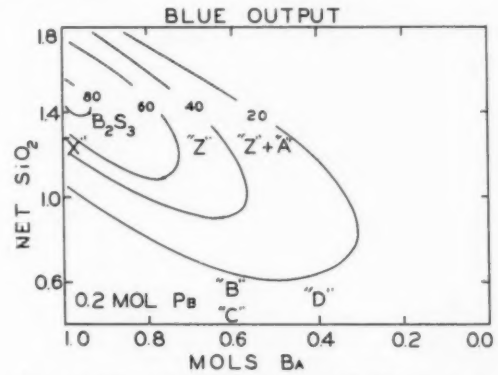

FIG. 15. Effect of SiO_2 content and Ba/Mg ratio on the blue output of barium magnesium lead silicates containing 0.2 mole PbO.

Field of 0.10 Moles PbO (Fig. 12 and 13)

Interesting changes in crystal structure and fluorescence are seen when the data of the preceding sections are plotted at constant lead content. The peak green output shown in Fig. 12 is associated with the presence of compound "Z," whereas barium mesotrisilicate is the predominant compound when the blue output is high.

As the composition is changed from 100 per cent BaO to 100 per cent MgO with 1.00 net SiO_2, we go from compound "X" to "Z" to a mixture of "Z" and "A" and finally to $MgO \cdot SiO_2$, whereas with low silica we obtain compound "C" at 50 per cent BaO, thus suggesting that "C" has the formula $BaO \cdot MgO \cdot SiO_2$.[4]

TABLE VII. *Barium magnesium lead silicate; mole composition and firing conditions for various types*

Type	Mole composition				Firing time (hr)/ temp °C	
	$BaCO_3$	MgO as basic $MgCO_3$	$PbCO_3$	Net SiO_2	Initial	Refiring
I	0.825	0.175	0.075	1.325	4/1000	4/760
II	0.70	0.30	0.10	1.05	4/960	4/760
III	0.60	0.40	0.20	0.90	4/900	4/760
IV	0.40	0.60	0.20	0.70	4/860	4/760

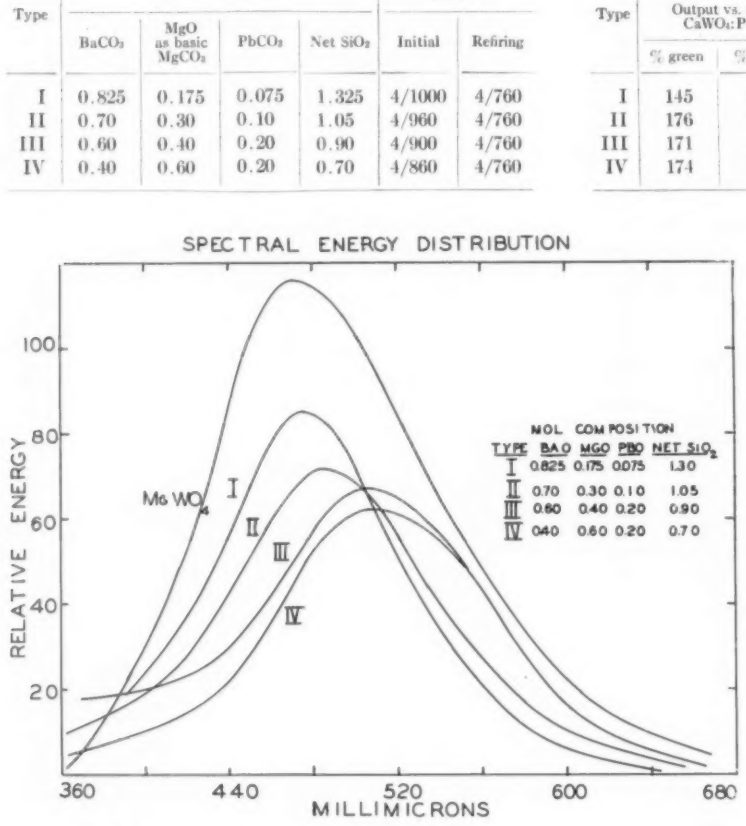

FIG. 16. Spectral energy distribution of certain barium magnesium lead silicates compared to that of magnesium tungstates.

Field of 0.20 Mole PbO (Fig. 14 and 15)

The results with 0.20 mole of PbO are much like those with 0.10 mole, but compounds "B" and "D" appear. Their location on the diagram gives the following speculative formula:

Compound	*Formula*
B	$PbO \cdot 3BaO \cdot 2MgO \cdot 4SiO_2$
D	$PbO \cdot 2BaO \cdot 3MgO \cdot 4SiO_2$

SPECIFIC PHOSPHORS

The preceding section has outlined the general behavior of the system and indicated four specific compositions which seemed sufficiently promising to warrant further study on a large enough scale to permit lamp tests.

The phosphor designated as Type I was quite thoroughly investigated, and small variations in composition, firing time, and firing temperature were tried. These variations raised the blue and green readings from 70 and 110, as shown in Fig. 2 and 3, to values of 82 and 150 for the best sample prepared. The optimum composition appears to be:

	mole
Barium carbonate	0.825
MgO (as basic magnesium carbonate)	0.175
Lead carbonate	0.075
Silicic acid, total	1.400
Silicic acid, net moles	1.325

Less extensive studies were made on Types II, III, and IV and the data below certainly do not represent the ultimate in output. Table VII gives the composition and firing conditions used in phosphor preparation, and Table VIII lists the output and the predominanting crystal structures.

TABLE VIII. *Barium magnesium lead silicate*

Type	Powder data				20 Watt lamp data	
	Output vs. std $CaWO_4$:Pb		sp gr	Crystal structure	0 Hour lpw	Coat. wt
	% green	% blue				
I	145	84	3.72	B_2S_3	24.8	3.4
II	176	70	4.00	B_2S_3	41.4	2.5
III	171	44	4.01	Z	35.6	2.6
IV	174	38	4.17	Z + A	33.1	2.0

[4] As suggested before, "A" may be a modification of "C."

The spectral energy distribution curves for the four specific types are given in Fig. 16 in comparison with magnesium tungstate. In general, the emitted light is blue-green in color with a low degree of saturation as would be expected from the wide spread through most of the visible spectrum.

Discussion

This preliminary survey of the system of phosphors formed by barium magnesium and lead combined with silicic acid to form complex silicates shows that two crystal structures give the best phosphors. The first of these is a modified barium mesotrisilicate containing about 10 mole per cent of lead, replacing barium. Magnesium can be substituted for barium up to nearly 30 mole per cent without appreciably changing the crystal structure, and, by careful control of composition, the fluorescence can be improved over the compound containing only barium. As this substitution is made the silica content must be reduced, and the hypothesis is put forward that barium and magnesium enter the lattice with different groupings around the silicon-oxygen tetrahedra.

The second type of crystal structure is that designated earlier as compound "Z." Several variants of this compound apparently fluoresce equally well, and a study of the diagrams shows that the best phosphors correspond rather closely to one of four definite mole proportions listed below:

BaO	*MgO*	*PbO*	*Total SiO_2*
1.0	—	1.00	2.0
1.0	0.25	0.75	2.0
1.0	0.67	0.33	2.0
0.67	1.00	0.33	2.0

In addition to these four variants of "Z," there appears to be another group of variants with excellent fluorescence having a lower cation content. These are:

BaO	*MgO*	*PbO*	*Total SiO_2*
0.50	0.66	0.50	2.0
0.66	0.50	0.50	2.0

Thus compound "Z" appears to be a mixed silicate of barium, magnesium, and lead in which the cation positions in the lattice are more or less interchangable and in which certain sites may also be left vacant.

Several other mixed silicates of more complex nature appear to exist, but do not have the strong fluorescence of the two simpler compounds discussed above.

Acknowledgments

We wish to express our appreciation to Mrs. V. M. B. Hannaford for her extremely careful identification of compounds in the complex powder patterns and to Mr. C. W. Jerome for preparation of some of the phosphors.

Any discussion of this paper will appear in a Discussion Section, to be published in the December 1950 issue of the Journal.

References

1. Keith H. Butler, *Trans. Electrochem. Soc.*, **91**, 265 (1947).
2. R. H. Clapp and R. Ginther, *J. Optical Soc. Am.*, **37**, 355 (1947).

Theory of Rate Processes as a Means of Studying Plating Reactions[1]

DONALD G. ROGERS AND ARTHUR A. BURR

Department of Metallurgical Engineering, Rensselaer Polytechnic Institute, Troy, New York

ABSTRACT

The application of modern theory of rate processes to plating cells has been discussed. Suggestions based on equations adapted from the literature have been made for a method of study of plating cells where current efficiency is less than 100 per cent and a procedure outlined involving current-voltage curves. Data collected for the plating of chromium from chromic acid show the applicability of the equations and indicate the possibility of this method of study for irreversible cells. The effect of sulfate ratio on the plating process has been studied by this method and data indicate that beneficial results from the sulfate ion result from a retardation of the hydrogen deposition rather than catalysis of the plating reaction.

INTRODUCTION

In a study of electrochemical processes, it may be said that three general types of reactions are encountered:

1. Those which reach approximate equilibrium conditions during operation.
2. Those which reach a "steady state" of operation at conditions considerably different from equilibrium but where the net rate of reaction becomes practically constant for a given set of operating conditions.
3. Those which may be referred to as transient type reactions where rates and concentration change appreciably with time.

When reactions of type 1 are encountered, the laws and equations of thermodynamics become sufficiently applicable to yield information of value in a study of the process. For reactions of type 2, recent developments in the mathematics of reaction rate theory due to Glasstone, Laidler, and Eyring (1) and others have supplied a method of attack. Reactions of type 3 are as yet difficult to interpret but are less frequently encountered in processes applied to production line methods.

Many processes, such as electroplating where a chain of reactions may be involved, consist of a combination of types 1 and 2. That is, one reaction in a complete mechanism may have a sufficiently slow reaction rate that it will allow the faster reactions involved to attain practical equilibrium conditions. If such processes are reversible and may be operated at a sufficiently slow rate to approximate equilibrium, thermodynamic calculations may be made. However, if for some reason this cannot be accomplished, the methods of rate theory must also be employed.

It is the purpose of the ensuing paragraphs to outline a possible method of utilizing the new rate theory as a tool for fundamental studies of plating reactions and to illustrate some of the possibilities of the method by experimental measurements on cells for plating chromium from chromic acid.

THEORY

Glasstone, Laidler, and Eyring (2) have shown that the current density through a cell is given by the relation:

$$I = \epsilon C_1 \frac{kT}{h} e^{\frac{-\Delta F_1^*}{RT}} e^{\frac{n\alpha wf}{RT}} \qquad (I)$$

which may also be written:

$$I = \epsilon C_1 \frac{kT}{h} e^{\frac{\Delta S_1^*}{R}} e^{\frac{-\Delta H_1^*}{RT}} e^{\frac{n\alpha wf}{RT}} \qquad (II)$$

where

C_1 is the concentration (or activity) of the depositing species in concentration units per unit area.
ΔF^* is the so-called free energy of activation.
ΔS^* is the entropy of activation.
ΔH^* is the heat of activation.
α is a fraction less than one and probably about 0.5.
w is the overvoltage for the deposition process, and is defined as the difference between the measured cathode voltage and the reversible voltage for the particular cell reaction under the given conditions of operation (see Fig. 2).
T is the absolute temperature.
ϵ is the value of the ionic charge.

[1] Manuscript received September 26, 1949. This paper prepared for delivery before the Chicago Meeting, October 12 to 15, 1949.

f is the Faraday constant.
k is Boltzman's constant.
h is Plank's constant.
R is the universal gas constant.
n is the valence change in the deposition process.

This equation is developed on the following major assumptions:

1. When a reaction takes place, the reactant molecules or ions must first reach an "activated state" or, in other words, they come together to form a loosely bound complex molecule which is referred to as the "activated complex." This will later decompose to form the reaction products. Such a process may be illustrated by an energy diagram of the type shown in Fig. 1.

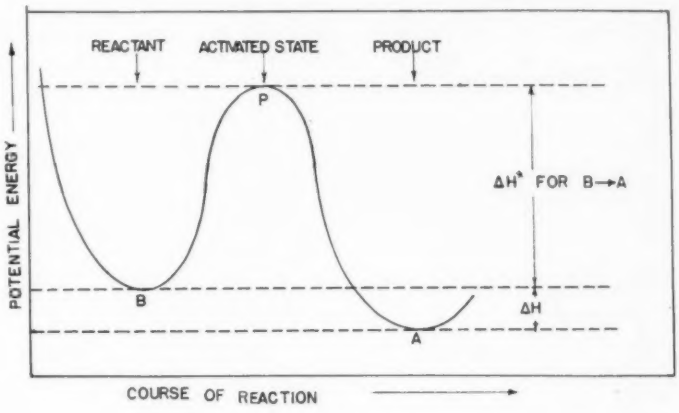

FIG. 1. Typical potential energy curve for a reaction B → A involving an activation energy

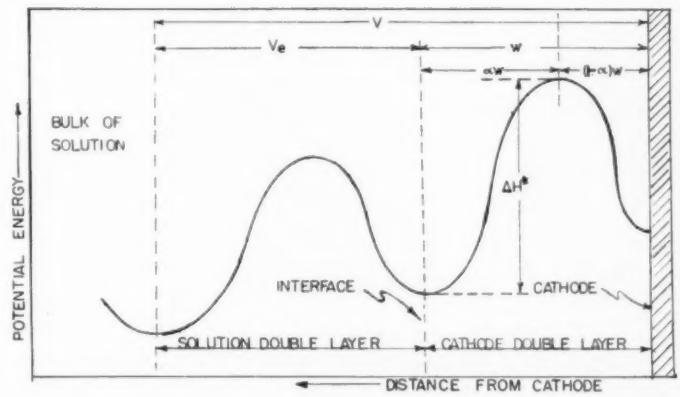

FIG. 2. Representation of double layers at the cathode surface.

2. In the process to which this equation is applied, the reverse or "deplating" reaction is negligible compared to the forward or deposition reaction. This holds true only when the overvoltage w is relatively large.

3. The fact that an overvoltage is required is explained by the postulated existence of a double energy barrier to be overcome in the deposition process. This is illustrated in Fig. 2. In this concept it is implied that under equilibrium conditions where the net current is zero, the difference in potential across the cathode double layer is zero and the difference in potential between the solution and the electrode is that across the solution double layer. When a resultant current flows in the cell, a potential difference across the cathode layer will be set up equivalent to the overvoltage for the particular operating conditions. If it is assumed that a reaction in the cathode double layer is the rate determining step, there will be no disturbance of the equilibrium across the solution double layer. The overvoltage will thus act in two ways to assist the plating reaction:

(*a*) Some fraction α may act to facilitate the plating reaction.
(*b*) A fraction 1- α will act to retard the deplating reaction.

Consequently the free energy of activation of the plating reaction is reduced by a quantity $-\alpha fw$. Since the deplating reaction is assumed to take place at a negligible rate for the conditions above, its effect may be neglected.

Using base ten logarithms, Equation (II) may be written in the form

$$\log I = \log \epsilon \frac{C_1 kT}{h} + \frac{0.43\Delta S_1^*}{R} - \frac{0.43\Delta H_1^*}{RT} + \frac{0.43n\alpha f}{RT}(V - V_e) \quad \text{(III)}$$

where V is the measured cathode potential and V_e is the corresponding equilibrium potential for the existing conditions.

Experimentally this means that for plating processes where overvoltage is high and current efficiency is near 100 per cent, a plot of log current density vs. cathode potential will be a straight line if the above assumptions are fulfilled. Each point on such a curve should, of course, represent sufficient operating time at the particular current density value to assure the attainment of "steady state" operation.

For the straight line portion of such a logarithmic current-voltage curve, the following conclusions may then be made:

1. For this portion of the operating range the rate of the process is being controlled by a reaction which is progressing at an appreciable but constant rate.

2. From the slope of the curve the value of the fraction α may be calculated according to the equation:

$$\frac{\partial \log I}{\partial V} = \frac{0.43n\alpha f}{RT} \quad \text{(IV)}$$

3. From data obtained at several temperatures, a series of log I values at constant V and varying T may be obtained. If a plot of log I vs. $1/T$ is then made, the slope of such a curve will be given by

$$\frac{\partial \log I}{\partial 1/T} = -0.43T - \frac{0.43\Delta H_1^*}{R} + \frac{0.43n\alpha f}{R}(V - V_e) \quad \text{(V)}$$

Since the effect of the first power temperature term should be small in the range of temperatures that can be covered and it may be assumed that ΔH^*, and V_e vary only slightly with temperature, this slope is relatively insensitive to temperature and the plot should be practically a straight line. From the value of the slope, the value of ΔH^* can be obtained.

4. Once the value of ΔH_1^* is established, the value of ΔS_1^* may be calculated if values for C_1 and V_e can be obtained. At least a number whose value will be dependent on ΔS_1^* can be established.

For processes where cathode current efficiency is appreciably less than 100 per cent, some changes must be made in the above equations. In general, it may be assumed that, if the plating process is taking place at low efficiency, other electrochemical changes are taking place at the cathode and utilizing electrical energy. This will result in two or more paths existing by which the electron current can be conducted from the electrode to the solution. It would seem reasonable to assume that this situation is analogous to a set of parallel electrical conductors and that the voltage drop across each conductor will, therefore, be the same. This will mean that the cathode potential measured as described below will be the V in the above equations for any of the processes. However, the measured current density for the cell will be divided among the cathode processes according to their relative conductivity which will, in turn, be dependent on their free energy of activation. Thus, if the current efficiency for the deposition reaction in a chromium plating cell is X per cent, Equation (II) becomes:

$$\frac{XI}{100} = I_{Cr} = \epsilon C_{Cr} \frac{kT}{h} e^{\frac{\Delta S_{Cr}^*}{R}} e^{\frac{-\Delta H_{Cr}^*}{RT}} e^{\frac{n\alpha wf}{RT}} \quad \text{(VI)}$$

This will not affect the value of α calculated from the slope of the current-voltage curve (except where current efficiency is changing rapidly with current density), but in calculating the value of ΔH_{Cr}^* the value of log I_{Cr} should be plotted. This will require a knowledge of the current efficiency values at each temperature and current density range.

Experimental

To obtain data for the application of these equations, a large number of accurately determined current-voltage curves are required. The measuring circuit used for this purpose is shown in Fig. 3. One inch (2.54 cm) square cathodes were used and cell currents were measured with a multi-range ammeter. Both copper and low carbon steel cathodes were used. Cathode potentials were measured by means of a calomel cell and salt bridge arrangement with the measuring tip in contact with the center of the cathode.

In order to be able to estimate when the cell had reached steady state operation under a given set of conditions, a recording potentiometer was used in conjunction with the ordinary hand operated potentiometer circuit. A small auxilliary circuit consisting essentially of a single 6SC7 tube was used to match the impedance of the recording potentiometer to the high impedance of the calomel cell and to avoid polarization of the cell or bridge due to excessive current drain. To assist in checking the reproducibility of the measurements, two plating cells in series were run simultaneously with two separate salt bridges

and calomel cells connected by a D.P.D.T. switch to the measuring circuit.

In starting a run, the two beakers containing the plating solution were placed in a constant temperature water bath. The cathodes were fixed in position above the solutions and the salt bridge tips properly placed with respect to the cathode. With the current turned on, the circuit was closed by elevating the water bath until the cathodes were submerged to the proper depth in the plating solution.

Solutions to be used were taken from a large stock supply of chromic acid prepared in advance. For each run, fresh solution was used and care was taken to keep all variables except those under study as nearly

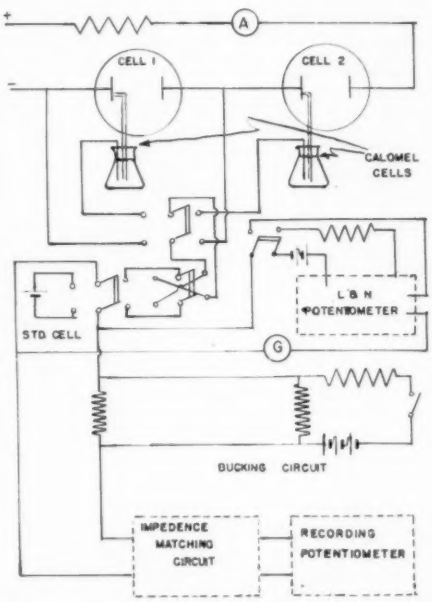

FIG. 3. Diagrammatic sketch of circuit used for determining current-voltage curves.

constant as possible. Curves shown are the average of numerous runs and each curve is plotted from approximately 25 points. In reproducing curves, only points indicating a change in slope are plotted to avoid confusion. For most runs, lead anodes approximately 3 square inches (19.4 cm^2) in area were used. Where high trivalent chromium content was required, iron anodes were used.

RESULTS AND DISCUSSION

Data for curves were obtained at 25, 45, 65, and 85°C. These curves are shown in Fig. 4. The solution was 2.5 molar chromic acid with 100:1 sulfate ratio and a trivalent chromium concentration of approximately 2 per cent. It will be noted that these curves, in general, consist of two major straight line portions with apparent transition regions and a sharp potential break. The upper region is the plating region, whereas in the lower region no plating takes place. The latter will be referred to as the "initial region." From these curves and the values of current efficiency for a chosen current density range, points may be obtained for a plot of log I_{Cr} vs. $1/T$ from which values of ΔH^*_{Cr} may be calculated.

Fig. 5 shows a series of curves at a constant temperature of 45°C and trivalent chromium content of less than 2 per cent obtained to show the effect of sulfate ratio. A similar series in Fig. 6 shows the effect of trivalent chromium content at a constant temperature of 45°C and 100:1 sulfate ratio.

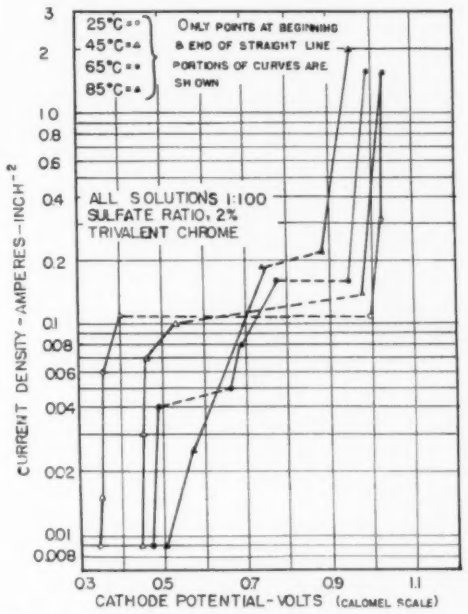

FIG. 4. Effect of temperature on current-voltage curves for 2.50 molar chromic acid.

The slope of the curves obtained for the initial region has been found so steep that no calculations have been attempted until more information can be obtained about the reactions taking place under these conditions. For the plating range, studies have been carried on to show the effect of sulfate ratio on the quantity ΔH^*_{Cr}. This required a series of curves similar to the upper part of Fig. 4 for each ratio studied. Values of log I were read at a constant value of V. Experimental values of current efficiency were determined in this operating range at each temperature and log I_{Cr} calculated. Fig. 7 shows a typical curve for log I_{Cr} vs. $1/T$ for a sulfate ratio of 100:1. A value of $V = 1$ volt (calomel scale) was used in obtaining these data although any suitable constant value of

V may be used. Table I shows a compilation of data from the study of sulfate ratio and Fig. 8 shows a plot of variations of ΔH^* with sulfate ratio. In making the calculations the mean value of $\frac{n\,\alpha\,f}{RT}$ was used and V_c was taken as 0.8 volt which is a rough average

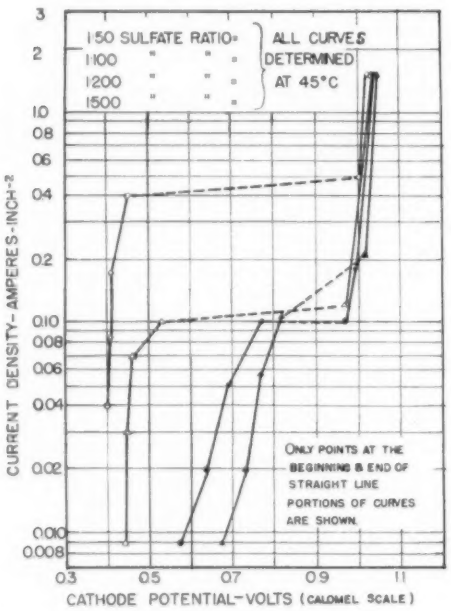
150 SULFATE RATIO
1100
1200
1500
ALL CURVES DETERMINED AT 45°C
CURRENT DENSITY- AMPERES-INCH-2
ONLY POINTS AT THE BEGINNING & END OF STRAIGHT LINE PORTIONS OF CURVES ARE SHOWN.
CATHODE POTENTIAL-VOLTS (CALOMEL SCALE)

FIG. 5. Effect of sulfate ratio on current-voltage curves in 2.50 molar chromic acid.

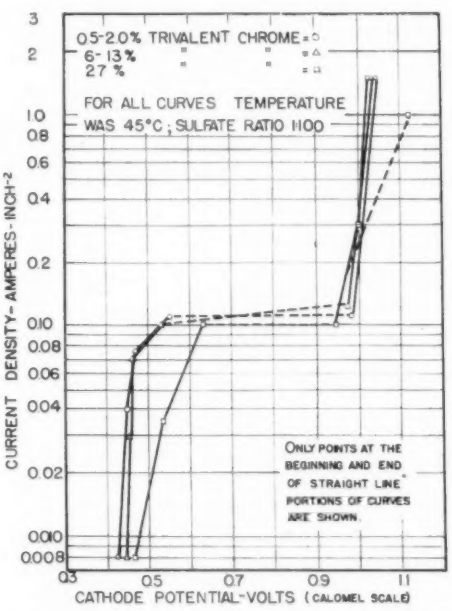
0.5-2.0% TRIVALENT CHROME
6-13%
27 %
FOR ALL CURVES TEMPERATURE WAS 45°C; SULFATE RATIO 1100
CURRENT DENSITY- AMPERES- INCH-2
ONLY POINTS AT THE BEGINNING AND END OF STRAIGHT LINE PORTIONS OF CURVES ARE SHOWN.
CATHODE POTENTIAL-VOLTS (CALOMEL SCALE)

FIG. 6. Effect of trivalent chromium concentration on the current-voltage curves in 2.50 molar chromic acid.

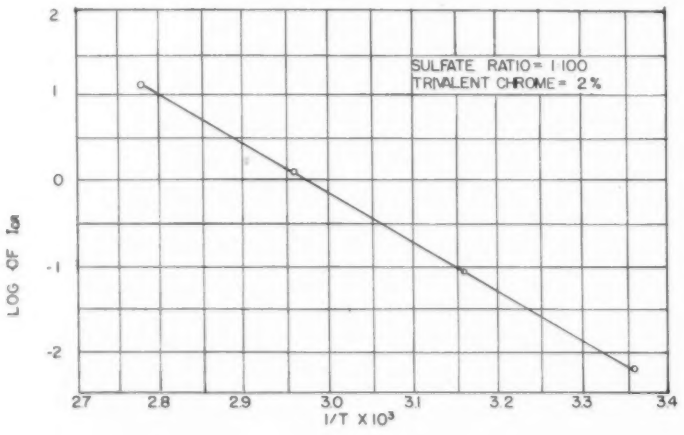

FIG. 7. Plot of log intercept vs. $1/T$ to determine ΔH^*.

of values in the literature for reversible chromium metal to ion couples.

To calculate ΔS^*, some value must be assigned to the quantity C_{Cr}, the number per square inch, in this case, of the depositing species. As a doubtful first approximation, one may assume homogeneous distribution of the reacting species according to the initial concentration (2.5M). This would give a concentration of 0.04 moles per cubic inch (.00244 moles/cm³) or approximately 25×10^{21} molecules per cubic inch (1.52×10^{21} molecules/cm³). This should give a distribution of approximately 10^{15} molecules per square inch (1.54×10^{11} molecules/cm²). If one assumes, with Glasstone, Laidler, and Eyring (3) that the solution molecules are packed with a distribution of 10^{15} molecules per square centimeter (or 6.5×10^{15} molecules per square inch) on the basis of molecule size and assumes further that the chromium concentration would vary as its mole fraction in solution, this gives a value of C_{Cr} of approximately

10^{14} molecules per square inch (1.54×10^{13} molecules/cm^2). The quantity $\epsilon \frac{kT}{h}$ is approximately 1×10^{-6} ampere-seconds which gives a value of 8 or 9 for the term $\log \epsilon C_{Cr} \frac{kT}{h}$. Using the values of ΔH^*, $n\alpha$, and I_{Cr} from the data on the plating reaction, the estimated values of ΔS^* and ΔF^* listed in Table I are obtained.

in the plating region values of $n = 2$ or 3 are more probable. This seems to indicate the possibility of a change in reaction mechanism in the deposition process depending on the current density range.

From Fig. 8 and the estimated values of ΔF^*, it may be said that these data indicate that the presence of the sulfate ion does not greatly affect the free energy of activation in the range of sulfate ratios commonly used in practice, but only shows an effect

TABLE I

Sulfate ratio	Temperature °C	$1/T \times 10^5$	Average current efficiency	$n\alpha$	Average $n\alpha$	Log I_{Cr}	V	ΔH^* cal	Estimated ΔS^* cal/deg	Estimated ΔF^* cal
50:1	25	336	27.8	3.7	2.9	−2.63	1.0	53,100	90	26,100
	45	316	17.4	2.3		−0.56				
	65	296	16.2	2.1		0.36				
	85	278	13.0	3.6		2.42				
100:1	25	336	24.6	2.0	2.0	−2.21	1.0	35,320	40	23,300
	45	316	13.0	2.0		−1.05				
	65	296	14.8	2.0		0.12				
	85	278	10.7	1.9		1.08				
200:1	25	336	24.6	2.0	1.5	−1.81	1.0	33,740	44	20,500
	45	316	7.1	1.5		−0.96				
	65	296	4.4	1.2		0.69				
	85	278	3.4	1.3		1.34				
300:1	25	336	21	1.8	1.6	−2.83	0.95	31,070	37	20,000
	45	316	6	1.9		−0.86				
	65	296	3.7	1.3		−0.58				
	85	278	2.9	1.1		0.11				

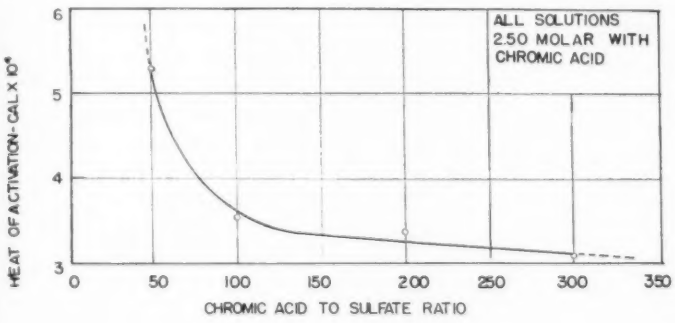

FIG. 8. Effect of sulfate ratio on the heat of activation (ΔH^*) of chromium.

The calculations of Table I are made for current densities above 1 ampere per square inch (.395 amp/cm^2). It was found that on most current-voltage curves a change in slope of the straight line portion occurs if measurements are made to relatively high current densities. Earlier calculations in the range from 0.1 to 1 ampere per square inch yield heats of activation in the neighborhood of 20,000 calories and entropies of activation of only a few calories for the 100:1 sulfate ratio.

It may also be noted that the values of $n\alpha$ given above indicate a value of around 0.5 for values of $n = 3$ or $n = 6$. However, for the lower current densities as the concentration of the sulfate ion becomes relatively high. This would seem to indicate that the beneficial effect of the sulfate ion is not as a catalyst for the plating reaction but probably as a retarder of the hydrogen deposition reaction. It may also be noted that the heats of activation listed in Table I are high compared to the average listed in the literature for the discharge of hydrogen ions (approximately 10,000 calories), which is in line with the relative rates of deposition of these two species at the cathode.

A few general remarks may be made regarding the initial region of the I-V curves. It follows more or less

logically from the theory that this region represents a different reaction or set of reactions than those occurring in the plating region. As no plating takes place, the cathode material may be expected to influence the results. This is, in fact, found to be true. Steel cathodes were found to give best reproducability but the slope of the straight line portion was found to be very steep with these cathodes. The authors believe that this range of variables represents a reduction reaction of hexavalent chromium ions to trivalent chromium ions together with possible evolution of a small amount of hydrogen. When a suitable overvoltage is reached at which the plating reaction may operate, a change in reaction mechanism will result with a corresponding rearrangement of the potential distribution at the cathode. Experiments are being carried out in an attempt to check these ideas and to try to find out whether the reactions of the initial region play any part in what takes place in the plating region.

Conclusion

In the analysis of many plating problems, a point is frequently reached where no measurable data can be found which can be related to the fundamental reactions of the process. This is particularly the case where the reactions involved are irreversible in the thermodynamic sense. The authors feel that the use of the reaction rate equations as illustrated above will supply new functions in ΔH^*, ΔS^*, ΔF^*, and the number α which are extensive properties of the reactions under study. Whether the absolute values or exact meaning of these quantities in the process can be definitely established seems doubtful at present, but, used on a comparative basis, they should be a valuable aid in relating experimentally measurable quantities of the plating cell to the reaction mechanism involved.

This conclusion is borne out for the data obtained so far for the chromium plating problem under study. At this time, the authors are not sufficiently satisfied with the experimental methods that they would like to make anything but tentative conclusions. These have already been presented in the discussion of data. The method of study is presented for the consideration and criticism of those who may be interested.

Acknowledgments

Many thanks are due to Dr. P. R. Kosting of the Watertown Arsenal Laboratory and other personnel of the Ordnance Department for helpful suggestions during the progress of the work.

Any discussion of this paper will appear in a Discussion Section, to be published in the December 1950 issue of the Journal.

REFERENCES

1. S. Glasstone, K. J. Laidler and H. Eyring, "The Theory of Rate Processes," McGraw-Hill Book Company, Inc., New York (1941).
2. *Ibid.*, p. 591.
3. *Ibid.*, p. 588.

Studies on the Structure of Hard Chromium Plate[1]

Cloyd A. Snavely and Charles L. Faust

Battelle Memorial Institute, Columbus, Ohio

ABSTRACT

The structural changes which take place during the annealing of chromium plate are illustrated by a series of photomicrographs. It is shown that recrystallization can be effected between 300°C (572°F) and 500°C (932°F). Loss of hardness is concurrent with recrystallization. A slight loss of hardness at lower annealing temperatures is ascribed to recovery from internal stress. The basis metal is shown to have an effect on the rate at which a growing electrodeposit assumes the normal preferred orientation.

The results of hydrogen extraction tests are given for temperatures up to 650°C (1202°F). X-ray and electron diffraction studies are presented to show that heating to above the temperature range at which the plate softens does not destroy the normal (111) preferred orientation.

Metallographic Studies

Introduction

The work reported in this section was undertaken to study the phenomena occurring during the annealing of "hard" chromium plate and to provide data for evaluation of existing theories for the hardness of "hard" chromium plate.

Two general concepts for the hardness of chromium plate have been published. One (1) accounts for it by the fine-grained condition of the plate, with internal stress being a minor contributing factor. Loss of hardness on heating is considered as resulting from recrystallization and grain growth. The other (2) accounts for hardness by a critical dispersion of chromic oxide particles which are said to exert a "keying" action to inhibit slip within crystals in a manner analogous to that postulated for various precipitation hardening alloys. Loss of hardness on heating is ascribed to agglomeration of the dispersed oxide particles with subsequent migration into the grain boundaries.

If softening is a result of recrystallization, then the beginning of major softening effects during annealing should be accompanied by the appearance of recrystallized grains in the metal. If softening is a result of agglomeration of oxides, these agglomerates should become sufficiently large after appropriate heat treatment to be visible under a microscope. Using this reasoning as a basis, a series of experiments was devised which involved plating hard chromium on steel cathode disks, annealing each of them at a different temperature, and subjecting all of them to metallographic examination.

[1] Manuscript received September 23, 1949. This paper prepared for delivery before the Chicago Meeting, October 12 to 15, 1949.

Experimental

All chromium plate samples used for the study were deposited from a bath containing 250 g/l (33 oz/gal) CrO_3 and 2.5 g/l (.33 oz/gal) SO_4. All samples but one were plated on ½-inch-diameter (1.27 cm) cathode disks of S.A.E. 4130 steel. One sample was plated [0.025 inch (0.0063 cm) thick] on a brass disk which could be easily dissolved away. The disks were held in a fixture (described in Reference 1) so that the peripheral surface and one side were masked, and the current density was reasonably even over the surface plated.

A series of specimens was plated for 24 hours at a current density of 250 amp/ft² (27 amp/dm²) and a bath temperature of 55°C (131°F). These were considered to represent standard hard chromium. Each specimen was halved with an under-water abrasive wheel. Half-disk specimens were then annealed in air at 500°C (932°F), 700°C (1292°F), 900°C (1652°F), and 1100°C (2012°F), respectively, for 12 hours. A specimen annealed at 300°C (572°F) was held at temperature for 22 hours. The annealed specimens were mounted in bakelite for polishing. Hardness measurements were made after polishing and etching for metallographic examination. A Tukon indentation hardness apparatus was used with a load of 100 grams and a reading magnification of 200×.

A single specimen was plated at a current density of 515 amp/ft² (55.6 amp/dm²), other conditions being the same as for the standard plate. This current density produced a nodular plate which was desired for comparison with the standard plate. This specimen, too, was cross sectioned. One half-disk section was annealed for 60 hours at 1100°C (2012°F) while buried in charcoal in a capped cast-steel container. This protection was necessary to

prevent complete oxidation of the steel basis metal during the treatment. The remaining half-disk section was not annealed. Both halves were then mounted for metallographic studies. The chromium plated on the brass disk was isolated by dissolving the brass in dilute nitric acid. The chromium disk which remained was treated in an air furnace at 1100°C (2012°F) for 68 hours. A black-green outer

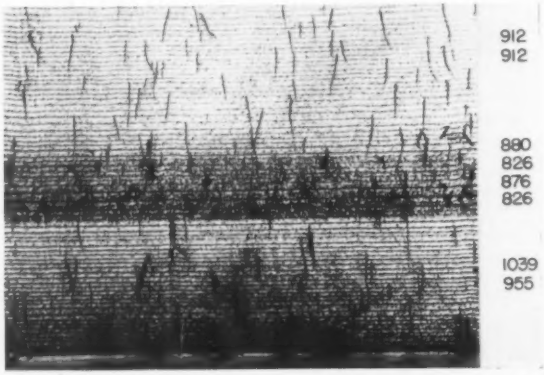

FIG. 1. Cross-sectional view of hard chromium plate in the "as plated" condition. Vertical lines are inclusion filled cracks. Horizontal lines are unexplained striations within the plate. Figures at right-hand margin are Knoop hardness numbers for the locations shown. HCl etch, approx. 200×.

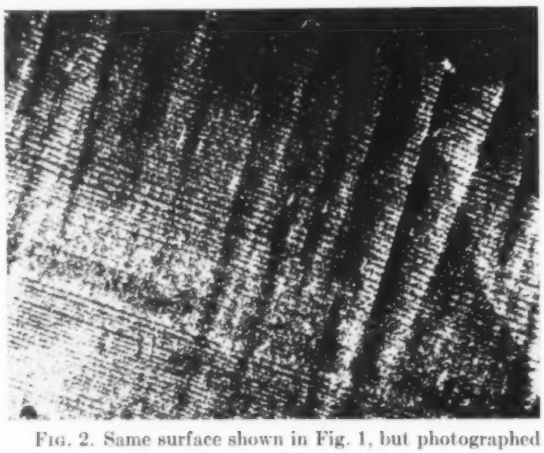

FIG. 2. Same surface shown in Fig. 1, but photographed with polarized light. The metallograph stage was rotated to the best position for revealing both striations and columnar structure. HCl etch, approx. 200×.

layer was then separated from the disk, leaving a metallic-appearing inner layer. These two materials were studied by x-ray diffraction for identification.

In the polishing operations, the mounted samples were taken through 4/0 metallographic paper by wheel and by hand, then rough polished on a silk cloth and finished on a medium-nap soft cloth. Metallographic-grade alumina was used on both cloths. Considerable difficulty was experienced in earlier attempts to reveal true structures when a billiard cloth was used for rough and finish polishing.

A concentrated (37%) hydrochloric acid etch was used throughout the metallographic work. No other etch was found to reveal the structure of the plate so well. However, this etch was far from ideal, often producing staining, or over- and under-etched areas on the same surface. It also tended to loosen inclusions from the etched surface. The etching was done at atmospheric temperature. The bakelite-mounted specimens were immersed in the etchant with the polished surface down for about 10 seconds.

Results and Discussion

The results of the annealing experiments are shown in Fig. 1 to 13. Fig. 1 shows the microstructure of a cross section of hard chromium plate in the

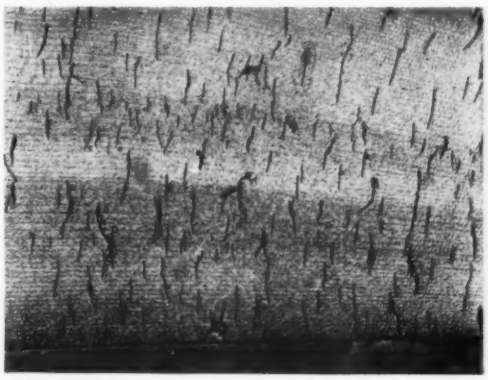

FIG. 3. Cross-sectional view of hard chromium plate after 22-hour treatment at 300°C (572°F). Striations are still visible although the etch did not bring them out as strongly as in the "as-plated" sample of Fig. 1. No evidence of recrystallized grains is visible. Figures at right-hand margin are Knoop hardness numbers for the locations shown. HCl etch, approx. 200×.

"as-plated" condition. The inclusion-filled cracks normally found in hard chromium plates are plainly shown in the photomicrograph. In addition, striations are shown which are not known to have been reported previously in the published literature. Examination of this surface at higher magnification did not reveal grain structure, though it was possible partially to resolve units elongated normal to the basis metal. Close inspection of the top center area of Fig. 1 reveals this type of structure. The numbers appearing at the right margin of Fig. 1 and succeeding figures are Knoop hardness numbers and will be discussed later.

Fig. 2 shows the same surface as Fig. 1, but illuminated with polarized light. In addition to the striations revealed in Fig. 1, the polarized light reveals columnar structures normal to the basis metal. These will be discussed in more detail later.

Fig. 3 shows a hard chromium plate after treatment at 300°C (572°F) for 22 hours. There is no indication that the heat treatment has caused any significant change from the structure shown in Fig. 1. The "dark etching" band shown in Fig. 1 does not appear in Fig. 3. However, it did appear in the specimen treated at 500°C (932°F).

Fig. 4 shows a hard chromium plate after treatment at 500°C (932°F) for 12 hours. Recrystallized grains are clearly revealed, thus definitely establishing that recrystallization of hard chromium plate begins between 300°C (572°F) and 500°C (932°F). Significantly, other investigators have shown effects relating to the volume shrinkage of plated chromium upon heating within this same temperature range. Hidnert (3) found that chromium plate may undergo

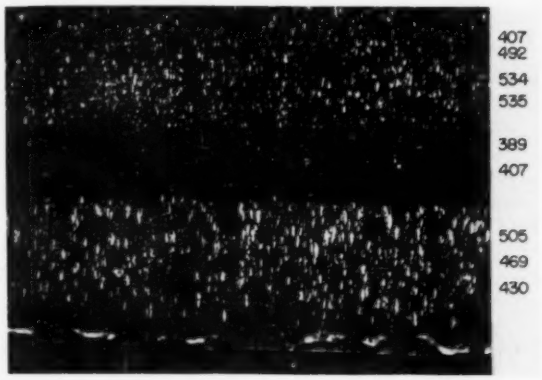

FIG. 4. Cross-sectional view of hard chromium plate after 12-hour treatment at 500°C (932°F). Recrystallized grains are plainly visible as the white elongated areas set in the darker background. Note that the striations are still faintly visible and that some of the recrystallized grains reach through several layers of striations. Figures at right-hand margin are Knoop hardness numbers for the locations shown. HCl etch, approx. 200×.

a volume shrinkage of approximately 2.5 per cent when heated to 500°C (932°F) for the first time. Wood (4) and Potter and Lukens (5) showed that the lattice parameter of chromium plate is normally somewhat greater than that of pure chromium and that heating to temperatures of 700°C (1292°F) and 500°C (932°F), respectively, did not completely remove the expansion. Heating to 1000°C (1832°F) did, apparently, destroy any effects which differentiated the parameter of chromium plate from that of chromium produced by nonelectrolytic methods.

Fig. 5 and 6 show hard chromium plates after treatment at 700°C (1292°F) and 900°C (1652°F), respectively, for 12 hours. Complete recrystallization of the plate occurred during the annealing treatment at 700°C (1292°F), and essentially no structural changes were effected by increasing the annealing temperature to 900°C (1652°F). However interdiffusion during the 900°C (1652°F) treatment produced an alloy layer between the steel basis metal and the chromium plate.

Fig. 7 and 8 show a cross section of the specimen annealed for 60 hours at 1100°C (2012°F). The surface shown was not etched, in order to retain clearly the effect on the oxide inclusions of prolonged

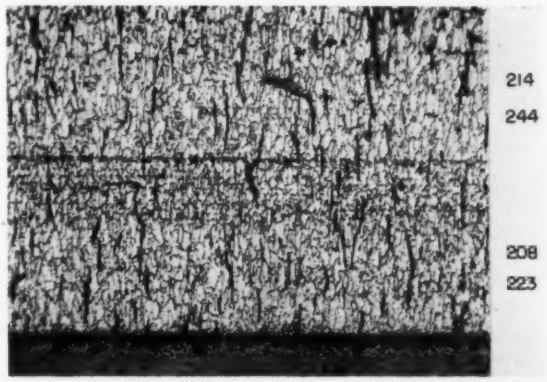

FIG. 5. Cross-sectional view of hard chromium plate after 12-hour treatment at 700°C (1292°F). The heat treatment has completely recrystallized the plate. Figures in right-hand margin are Knoop hardness numbers for location shown. HCl etch, approx. 200×.

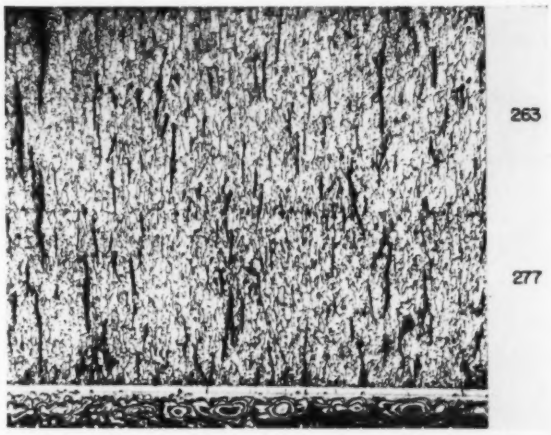

FIG. 6. Cross-sectional view of hard chromium plate after 12-hour treatment at 900°C (1652°F). Little or no change from the structure of Fig. 5 (700°C annealing) has occurred. Note that an alloy layer has formed between the steel basis metal and the chromium plate. Figures in right-hand margin are Knoop hardness numbers for the locations shown. HCl etch, approx. 200×.

annealing at high temperature. The inclusions as shown in Fig. 1 are known to be a hydrated chromium-oxygen combination which forms Cr_2O_3 when dehydrated by heating (6). Fig. 7 and 8 show that, when these inclusions are subjected to a high-temperature [1100°C (2012°F)] anneal, they separate into numerous globules or spheroids of oxide which lie along the location of the original void in the plate.

The "dispersed-oxide" theory states that the oxide in the inclusions visible in "as-plated" chromium (as in Fig. 1) is but a small portion of the total oxide present in the plate. Close inspection of Fig. 7 and 8 leads to the conclusion that a major portion, if not all, of the oxide visible after annealing occupies approximately the same positions of the original inclusions and, therefore, it may be assumed to have originated in these positions.

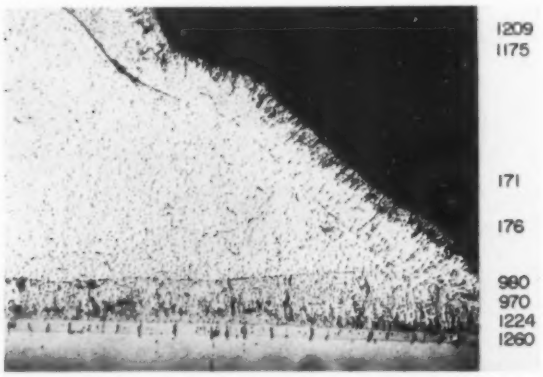

FIG. 7. Cross-sectional view of hard chromium plate annealed at 1100°C (2012°F) for 60 hours. The separate layers shown are, from the bottom up: steel basis metal, iron-chromium diffusion layer, chromium nitride layer, recrystallized chromium plate, and chromium nitride. The chromium nitride layer surrounds the recrystallized chromium plate on all sides. Figures in right-hand margin are Knoop hardness numbers for successive layers. As polished, approx. 50×.

X-ray diffraction data for the unbacked, annealed chromium plate sample are shown in Fig. 9, along with standard data from the literature for comparison. The green-black outer layer was identified as chromic oxide (Cr_2O_3). The inner layer was identified as the hexagonal chromium nitride (Cr_2N) with some B.C.C. chromium metal also present.

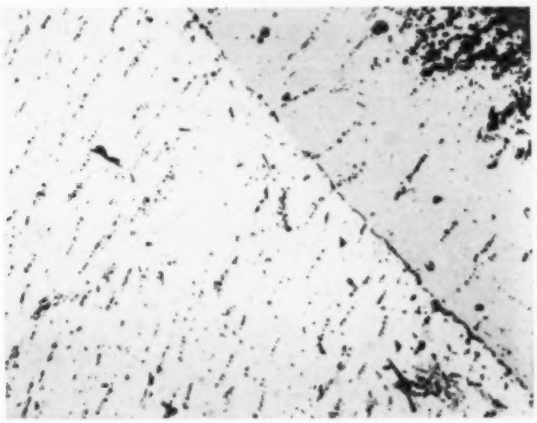

FIG. 8. Same plate shown in Fig. 7. View shown is at boundary between recrystallized chromium plate (lower left) and chromium nitride (upper right). Note that major portion of the oxide particles are globules strung out in lines, indicating that they are probably dehydrated inclusion films. As polished, approx. 160×.

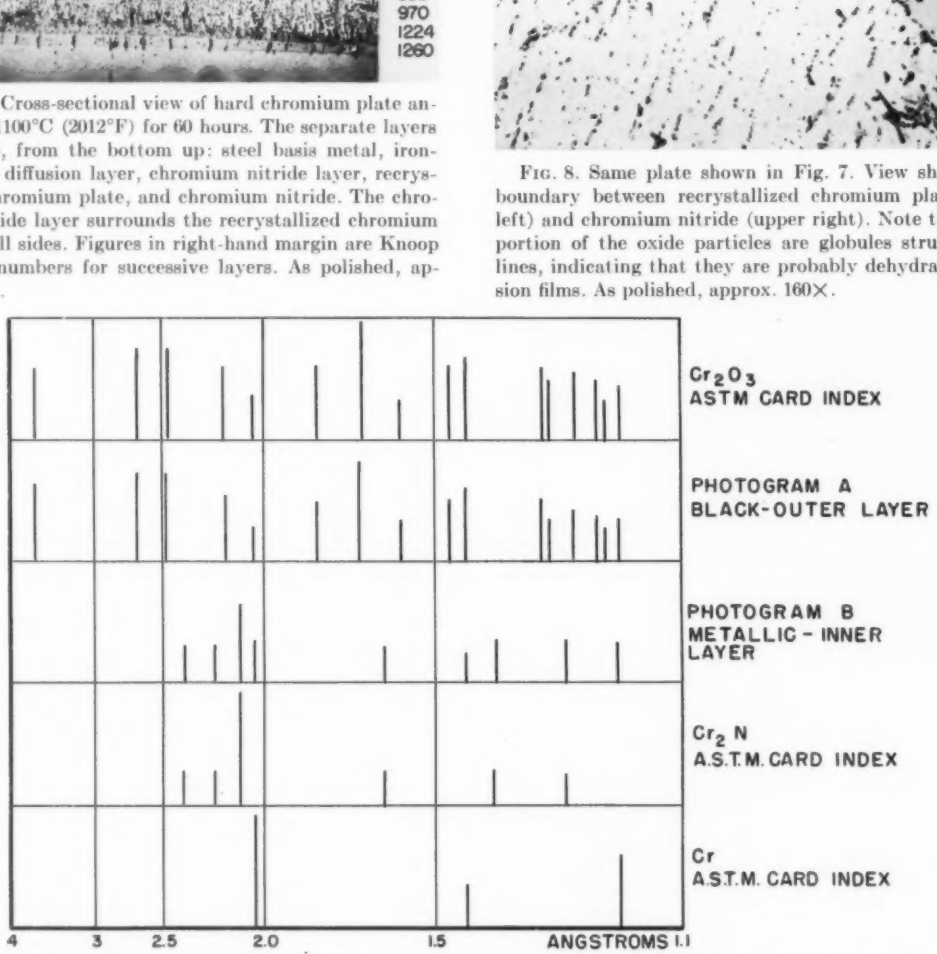

FIG. 9. Graphical representation of x-ray diffraction data. The abscissae represent interplaner spacings in ångström units. The ordinates represent the relative intensities.

Similarity between the identified phase and the layer surrounding the chromium in Fig. 7 and 8 led to the conclusion that this layer, too, is Cr_2N. It

appears both at the plate surface and at the plate-steel interface, indicating that nitrogen was drawn from the steel, as well as from the air.

Apparently, air oxidation of chromium at both moderate and elevated temperatures is slow because of the density of the oxide film that is formed. However, at temperatures in the region of 900°C (1652°F) or above, a nitride of chromium is readily formed, regardless of the surface film of oxide. The nitrogen atom appears to penetrate the oxide film to reach the underlying chromium metal. Modern theory for the mechanism of oxidation holds that, in some cases, metal atoms must diffuse through covering oxide films to the air-oxide interface if additional oxide is to be formed. The large size of the oxygen atom is considered to prevent its penetration into the oxide to reach the underlying metal. Following the same reasoning, the small size of the nitrogen atom may explain the ease with which it penetrates the oxide film to form chromium nitride.

It is surprising that so much of the nitride phase was formed on the chromium annealed in charcoal. Evidently, chromium will form nitrides, if the temperature is sufficiently high, even though the concentration of nitrogen is very low. A similar situation is known to exist between chromium and oxygen at lower temperatures, although, in that case, the initial reaction product is a protective film.

No attempt was made to determine the exact composition of the "third phase" shown in Fig. 7, i.e., the layer between the nitride shell and the steel basis metal. This material is believed to be a diffusion alloy of iron and chromium with the possibility that the chromium is a nitride. The hardness of 1200–1275 Knoop indicates that the material may have interesting properties for engineering applications.

Fig. 10 shows a cross-sectional view of hard chromium plate annealed at 1100°C (2012°F) for 12 hours. Nitrogen from the air has penetrated the crack in the plate to form a layer of nitride along each wall of the crack. The 1100°C temperature has produced nearly equi-axed grains as compared to the elongated grains of Fig. 5 and 6. The oxide inclusions remain "in situ" with no indications of a tendency to migrate to the grain boundaries.

Fig. 11 and 12 show cross-sectional views of an unannealed portion of the chromium plate shown in Fig. 7 and 8. The relation of the striations to the plate surface is clearly shown. The "dark-etching" area is an anomaly. A similar area is noted in the plates of Fig. 1, 4, 5, and 6, and was observed in numerous other instances. The presence of such "dark-etching" areas in chromium plate has been mentioned[2] by other workers, but has not been reported in the literature. No explanation for these areas is now available. It is hoped that further con-

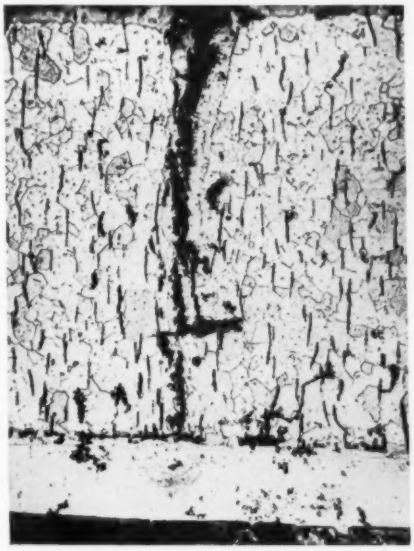

FIG. 10. Hard chromium annealed at 1100°C (2012F) for 12 hours. Grains have now become nearly equi-axed. Inclusions are clearly shown to be in original positions with no evidence of mitration into grain boundaries. Note the nitride penetration along the large vertical crack in the plate. HCl etch, approx. 140×.

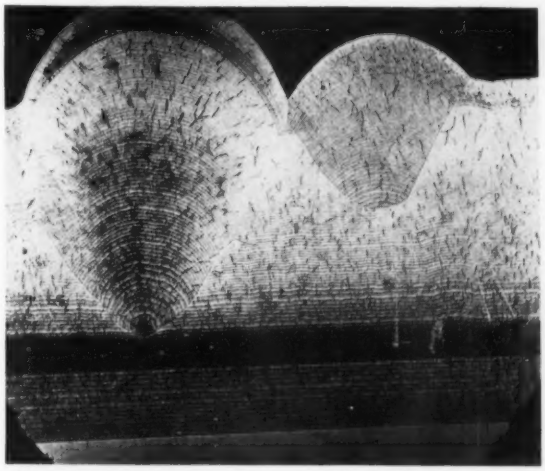

FIG. 11. Cross-sectional view of "as-plated" portion of plate shown in Fig. 7 and 8. A high current density was used to deposit a nodular plate. The etch has revealed the striations which apparently correspond to the various levels of the surface as the plating was in progress. Compare with Fig. 1 which shows a plate deposited at normal current density. HCl etch, approx. 50×.

[2] Mentioned by Lt. (j.g.) J. H. James, U.S.N., of the Naval Aviation Material Center, Philadelphia, Pennsylvania, during a conversation with one of the writers.

sideration will allow explanation of this puzzling structural characteristic.

Ordinary light was used to illuminate the specimen in Fig. 11. Polarized light was used for Fig. 12 and the columnar mode of growth is strikingly illustrated.

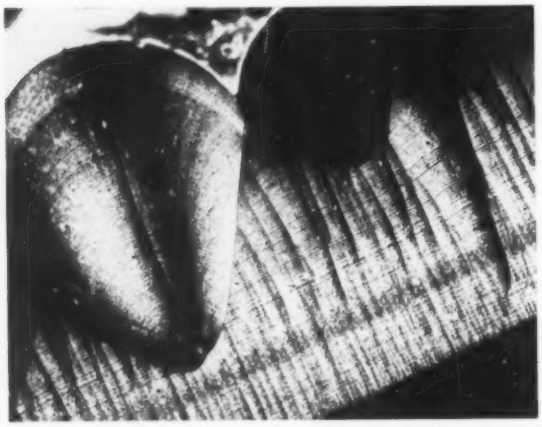

FIG. 12. Same surface as shown in Fig. 11, but illuminated with polarized light. The mode of growth of nodules is revealed. The metallograph stage was rotated from the position of Fig. 11 to the best position for revealing both striations and nodules. Compare with Fig. 2. HCl etch.

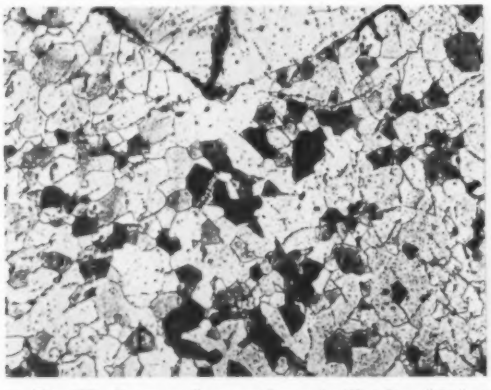

FIG. 13. Same surface as shown in Fig. 7 and 8, but after HCl etch. Equi-axed grains of recrystallized chromium are now revealed. Grains are also revealed in the nitride phase at the top. The positions of oxide inclusions are not so clearly shown here as in Fig. 9. Knoop hardness numbers for the recrystallized chromium are given in the right-hand margin. HCl etch, approx. 200×.

Apparently, each of the "columns" represents an individual nodule or "dome" growing on the plate surface. The occurrence of such domes on the surface of chromium plate has been reported by numerous observers.

Since the chromium crystals are B.C.C. and, therefore, isotropic, the effect of polarized light is surprising. However, the crystals are known to be oriented, and the mode of recrystallization, shown in Fig. 4, leads to the suspicion that the as-plated crystals, though small, are elongated normal to the plate surface. Limited studies with the electron-microscope have strengthened this suspicion. In addition, the plate is stressed, and is restrained only in the plane of the basis metal. This combination of circumstances, or a part of them, may cause the partial extinction of polarized light.

Fig. 13 shows the specimen of Fig. 7 and 8 after etching with hydrochloric acid. The positions of inclusions as revealed in Fig. 8 have now been somewhat obscured by the etch. If Fig. 8 were not available, Fig. 13 could be misinterpreted as showing that a major portion of the inclusions has migrated to grain boundaries. The grain structure of the chromium nitride phase has been brought out by the etch. It is possible that the chromium nitride could be mistaken for recrystallized chromium. Such a misinterpretation was made in this work until proper polishing and etching techniques were found for revealing the true structure.

The Knoop hardness numbers, given at the sides of the various Figures, indicate the progress of softening as related to the changes in microstructures shown. These data show that temperatures of the order of 1000°C or over are necessary to obtain complete or "dead" annealing in twelve hours or less. The softness of the annealed material makes it very difficult to polish for metallographic examination because of the tendency to drag metal into scratches. This loose metal is then rapidly attacked by the etchant, showing the surface to be imperfectly polished.

The hardness measurements, reported herein, were made on cross sections of the plates. These measurements are at variance with others taken on the surfaces of plates similarly treated. X-ray studies have shown that chromium plates are highly oriented [(111) planes parallel to the surface of the basis metal]. The indications are that the hardness of a given plate may vary by as much as 200 Knoop numbers depending on the direction of measurement.

These results support the theory that softening of chromium plate is related to recrystallization and grain growth in the plate. The dispersed-oxide theory is not supported, and some of the evidence directly contradicts that theory.

The appearance of the columnar structures in chromium plate observed under polarized light indicates that, regardless of the fine-grained character of the plate, the influence of the first layer deposited is carried throughout the plate. The regularity of the bands, or striations, and their continuity across the plate indicate a periodic phenomenon for which the authors have no precise

explanation. The thickness of the striae indicates a periodic cycle of approximately fifteen minutes. It is difficult to conceive of a cyclic phenomenon occurring in the plating solution, or in the cathode film, with so long a period. Preliminary studies with the electron microscope at 5000× have shown that the grains, or crystalline aggregates, are elongated normal to the base metal, and that successively larger aggregates are formed as the plate builds up. Suddenly, the plating surface is entirely covered with small aggregates and the growth cycle is repeated. Much additional data are needed for an adequate explanation of the facts of the case.

X-ray and electron diffraction studies were used to identify the orientation, or lack of it, in each specimen. The results are presented in Table I. They indicate that the cubic crystals comprising chromium plate are distributed in random positions in thin plates. In thick plates, the crystals are arranged, or oriented, with the (111) plane parallel to the plate surface. As plating proceeds, the random arrangement changes to the regular "parallel to surface" arrangement. Plates on cold-rolled brass and on electropolished steel achieve the "parallel-to-surface" arrangement much more quickly than do those on machine-ground steel.

TABLE I. *Effect of plate thickness and of basis-metal surface on the crystal orientation of bright chromium plate**

Sample No.	Basis-metal surface	Plating time (min)	X-ray results	
			Pattern identified and intensity	Crystal orientation‡
1	Machine-ground steel†	5	Chromium—medium	Random
2	" "	10	Chromium—medium	Random
3	Brass	5	Chromium—weak, brass—weak	Chromium—random + brass—oriented
4	"	10	" " " "	Chromium—weakly oriented + brass oriented
5	"	15	Chromium—weak	Oriented
6	"	20	Chromium—very weak	Oriented
7	Machine-ground steel	15	Chromium—weak + steel?	Random
8	" "	20	Chromium—weak	Random
9	Electropolished steel	5	Chromium—strong + steel?	Random
10	" "	10	Chromium—weak	Weakly oriented
11	" "	15	" "	" "
12	" "	20	Chromium—very very weak	Weakly oriented

* All plating done in 250 g/l CrO_3 bath with $\frac{100}{1}$ acid ratio, at 130°F, and with a current density of 300 amp/ft² (33 amp/dm²).

† SAE-4130 steel was used.

‡ By means of electron diffraction tests, the preferred orientation was identified as (111) plane parallel to the basis-metal surface.

The Effect of the Basis Metal on the Crystal Orientation of Chromium Plate

A short series of experiments was performed to identify any effect of the basis-metal surface on the structural make-up of chromium plated on it. Numerous investigators have shown that chromium plate is normally oriented with the (111) plane parallel to the basis metal. However, whether this orientation was assumed at the very beginning of plating or at some time during build-up of a plate was not established. Any effect of the surface character of the basis metal also remained unidentified.

Samples of bright chromium were plated on one side of one-half-inch disks of cold-rolled brass, electropolished steel, and machine-ground steel. Plating periods of 5, 10, 15, and 20 minutes were used for each type of surface, making twelve specimens in all.

From these data, the deduction is that the surface of ground steel is so rough and broken that deposition must continue for a considerable time to achieve the (111) preferred orientation normal for chromium plate. The brass surface consisted of at least partially oriented crystals, so a relatively short plating time of 10 minutes produced an oriented plate. Electropolished steel, similar to the brass, allowed the chromium plate to achieve the preferred orientation after 10 minutes of plating.

All chromium plates are indicated as likely to be oriented if plating is continued to build up thick deposits. The preferred orientation is quickly achieved if the basis-metal surface is smooth and regular. If the basis surface is irregular, as a result of grinding or machining operations, plate thicknesses over 0.0005 inch (.0127 mm) must be reached before any considerable degree of preferred orientation is found.

Samples of hexagonal chromium hydride were then plated on the same three types of basis-metal surface using previously described (1) techniques.

They were examined with the x-ray spectrometer immediately after plating. Within the sensitivity of the spectrometer measurements, the plates were entirely hexagonal hydride. The crystal size was computed to be about 10^{-5} cm for each plate.

The hydrides were then decomposed by treatment for 1 hour at 150°C (302°F) in an air oven. patterns were very broad. No estimation of the grain size was possible because of the similar effects of internal stress and fine grains to cause broadening of x-ray pattern lines. Special stress measuring methods might allow definition of the two separate effects.

The plate on electropolished steel was treated at 250°C (482°F) for 1½ hours. It was again x-rayed and the pattern was no different than that obtained after the 150°C (302°F) treatment. The hardness of the

TABLE II. *Data obtained during experiments with the decomposition products of electrodeposited hexagonal chromium hydride*

Sample No.	Basis-metal surface	Plating* time (hrs)	Grain size for hydride	Crystal† orient. after heating	Adherence after heating	Hardness‡ after heating
			cm			
14	Steel ground	3	10^{-5}	Random	Cracked and separated	—
21	Steel electropolished	4.5	10^{-5}	Random	Adherent	419—avg. (Knoop)
22	Brass rolled	3.5	10^{-5}	Random	Cracked and partly separated	—

* All plates deposited from bath containing 589 g/l total Cr calculated as CrO_3, $\frac{200}{1}$ acid ratio, and with 15.7 per cent of the Cr in the Cr^{+3} state. Bath temperature = 4°C, current density = 185 to 200 amp/ft² (19-21 amp/dm²).

† The samples were heated for 1 hr at 150°C to decompose the hydride, forming body-centered cubic Cr.

‡ The hardness was measured after a 1½-hr treatment at 250°C, in addition to the hour at 150°C.

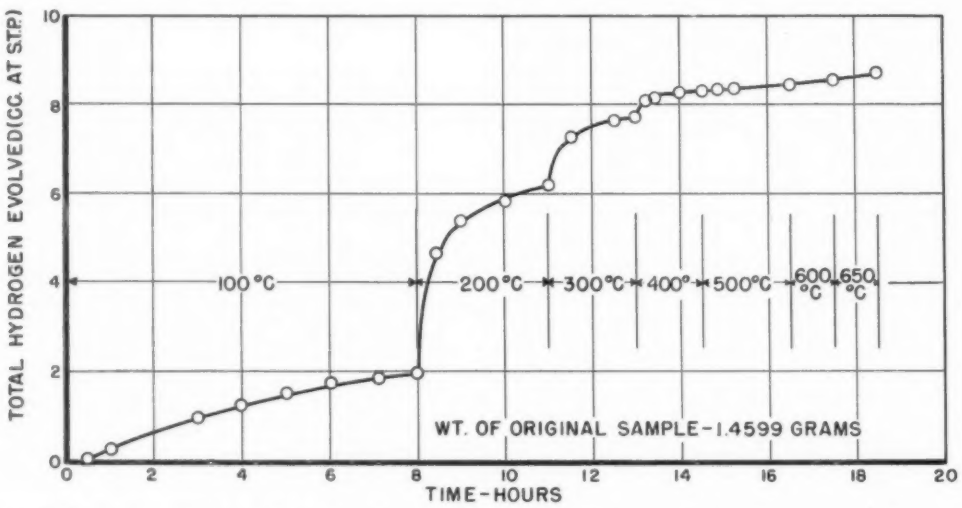

FIG. 14. Hydrogen volume given off by chromium plate subjected to temperature-time increments under vacuum

During the treatment, the plates separated from the ground steel and brass basis-metal disks. The sample on the electropolished steel backing showed no tendency to separate. In previous work of a similar nature with brass backings, no separation difficulties were encountered, so the adhesion must have been unusually poor in this case.

The decomposed hydrides were x-rayed again and found to be bodycentered cubic crystals with random orientation. Table II presents the data obtained in this series of tests. The lines of the x-ray

sample was then found to be 419 Knoop (500-g load and 200× reading magnification).

Hydrogen in Chromium Plate

A sample for hydrogen extraction tests was prepared using the 250 g/l (33 oz/gal) CrO_3 solution and the plating conditions described in the previous section. Six brass disks were used as cathodes and they were subsequently dissolved in dilute nitric acid, leaving the chromium plates unattacked. The six chromium disks weighing 1.4599 grams were

placed in a gas extraction apparatus (7) and brought to the specified temperature while under vacuum. The evolved gas was captured, measured, and analyzed to make certain it was essentially pure hydrogen. Treatment at each of the various temperatures was continued until the gas evolution slowed down considerably. The volume of evolved gas was read at frequent intervals for each treatment temperature. These data, presented in Fig. 14, agree fairly well with those of Makariewa and Birukoff (8), and Potter and Lukens (5).

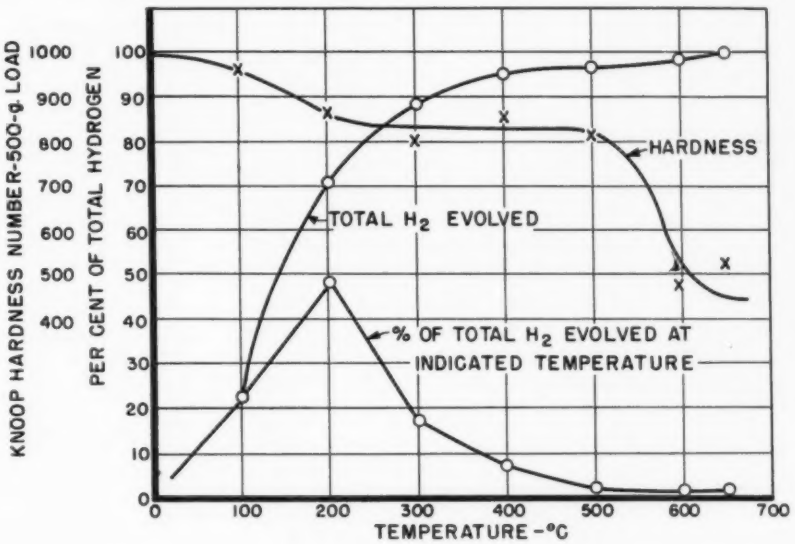

FIG. 15. Hydrogen evolved from chromium plate during vacuum-temperature treatments, and the hardness of the plate after the treatments.

It is significant that the chromium studied by Potter and Lukens was deposited from a trivalent chromium bath according to the Bureau of Mines electrowinning process, and that material was essentially no different from the plate from the chromic acid bath investigated in the present work.

Effect of Vacuum Heat Treatment on the Hardness and Crystal Orientation of Chromium Plate

Brass disks, ½ inch (1.27 cm) in diameter, were plated with chromium on one side only under conditions identical to those used for the preceding sections. Plating time was four hours. The samples were then subjected to vacuum-temperature treatments as shown in Table III. The time of treatment at each temperature was chosen by consulting Fig. 14 to reach an estimation of the time required to extract a major portion of the gas possible of removal at that temperature. At temperatures of 100°C (212°F) and 200°C (392°F), the indicated time was excessive, so treatments of 60 minutes were adopted as a compromise. After each temperature treatment was completed, a sample was withdrawn from the extraction apparatus and held for x-ray, electron diffraction, and hardness tests.

The samples treated at 500°C (932°F) and above were covered with a visible oxide film after the treatments. Following the x-ray examination, these samples were prepared for electron diffraction tests by polishing lightly with worn No. 600 metallographic abrasive paper and then with levigated alumina on a billiard-cloth lap. A light hydrochloric acid etch was the final step.

TABLE III. *Effect of vacuum heat treatment on hardness and crystal orientation* in bright chromium plate†*

Sample No.	Vacuum heating temp (°C)	Time‡ at temp (min)	Average hardness§ (Knoop)	Number of hardness measurements
z 13	100	60	961	4
15	200	60	864	4
16	300	60	803	5
17	400	30	856	4
18	500	30	816	4
19	600	30	486	1
20	650	30	524	2

* Electron diffraction tests showed that all of the above plates were oriented with the (111) plane parallel to the basis.

† All plates on brass, 250 g/l CrO_3 and $\frac{100}{1}$ acid ratio solution, 130°F, 300 amp/ft² (33 amp/dm)², plating time—3½ hr.

‡ Time at temperature is cumulative. Each specimen received all treatments listed above it.

§ 500-g load, 200× magnification for reading impression.

The results of these tests and of the previous hydrogen extraction tests are shown in Fig. 15. The curve shown for the hardness vs. temperature relation is believed to be the best approximation possible

from these data and from published data available. The form of the curve (9) indicates that two separate effects may be taking place as the temperature of treatment is increased. First, at temperatures up to 300°C (572°F), stress relief is thought to explain the softening. The increased movement of the atoms necessary for stress relief probably also accounts for the escape of hydrogen from the plate. The rapid decrease in hardness on heating over 500°C may be ascribed to recrystallization and grain growth in the plate. It should not be assumed that serious softening will not occur below 500°C (932°F). The curve shown applies only to the heating periods used in these tests and longer periods would undoubtedly produce softening at lower temperatures. No change in crystal orientation was found, regardless of the recrystallization believed to have occurred during the treatments at temperatures over 500°C (932°F).

Acknowledgements

The assistance of various members of the Battelle Memorial Institute staff is gratefully acknowledged: C. M. Schwartz and D. A. Vaughan for the x-ray and electron diffraction tests and interpretation; M. V. Mallett for the gas extraction work.

The research reported herein was carried out under the sponsorship of the Army Ordnance Department. This financial support and the active interest of Army Ordnance technical representatives is gratefully acknowledged.

Any discussion of this paper will appear in a Discussion Section, to be published in the December 1950 issue of the JOURNAL.

REFERENCES

1. C. A. SNAVELY, *Trans. Electrochem. Soc.*, **92**, 537 (1947).
2. A. BRENNER, P. BURKHEAD, AND C. W. JENNINGS, *Proc. Am. Electroplaters' Soc.*, **34**, 32 (1947).
3. P. HIDNERT, *J. Research Nat. Bur. Standards*, **26**, 81 (1941).
4. W. A. WOOD, *Phil. Mag.*, **23**, 984 (1937).
5. E. V. POTTER AND H. C. LUKENS, *Trans. Am. Inst. Mining Met. Engrs., Metals Technol.*, **15**, No. 1, Tech. Pub. 2312 (1948).
6. J. B. COHEN, *Trans. Electrochem. Soc.*, **86**, 441 (1944).
7. The apparatus was similar to that described by W. C. NEWELL, *J. Iron Steel Inst. London*, **141**, 243 (1940).
8. S. P. MAKARIEWA AND N. D. BIRUKOFF, *Z. Elektrochem.*, **41**, 623 (1935).
9. The general shape of the curve is very similar to that shown by T. C. JARRETT, *S.A.E. Journal*, **52**, 222 (1944).